ELSEVIER

Chemical Geology 227 (2006) 236–257

CHEMICAL GEOLOGY
INCLUDING
ISOTOPE GEOSCIENCE

www.elsevier.com/locate/chemgeo

Geochemical signature of Paleozoic accretionary complexes of the Central Asian Orogenic Belt in South Mongolia: Constraints on arc environments and crustal growth

Christoph Helo [a,*], Ernst Hegner [a], Alfred Kröner [b], Gombosuren Badarch [c], Onongin Tomurtogoo [c], Brian F. Windley [d], Peter Dulski [e]

[a] *Department für Geowissenschaften, Universität München, Theresienstraße 41, 80333 München, Germany*
[b] *Institut für Geowissenschaften, Universität Mainz, Becher-Weg 21, 55099 Mainz, Germany*
[c] *Institute of Geology and Mineral Resources, Mongolian Academy of Sciences, Enk Taivam Ave. 63, Ulaanbaatar 210351, Mongolia*
[d] *Department of Geology, University of Leicester, University Road, Leicester LE1 7RH, UK*
[e] *GeoForschungsZentrum Potsdam, Telegrafenberg A-50, 14473 Potsdam, Germany*

Received 4 April 2005; received in revised form 1 September 2005; accepted 11 October 2005

Abstract

We report a reconnaissance geochemical and Nd-isotopic study for 33 metaigneous and metavolcaniclastic rocks from the ca. 470 to 290 Ma old Gurvan Sayhan, Zoolen, Nemegt Uul, Bayanleg-Hatuu, and Tseel mountain ranges in southern Mongolia, in order to infer tectonic environments, test a recently proposed multiple terrane model, and explore the late-stage development of the southern Central Asian Orogenic Belt (CAOB). Samples from the Gurvan Sayhan and the Zoolen ranges have a predominantly intermediate, calc-alkaline composition; they display LREE enrichment, excess abundances of fluid-soluble elements, and low concentrations of high-field strength elements. These data, in combination with high initial ε_{Nd}-values of ca. +5 to +9, are consistent with a juvenile intra-oceanic arc. Some of the samples are chemically similar to adakites and high-Mg andesites and thus predictably evolved in forearc settings. The Gurvan Sayhan and Zoolen ranges have previously been considered as an island arc and accretionary prism, respectively. However, our data show indistinguishable, mutual, geochemical characteristics suggesting that both areas were part of a single intra-oceanic island arc-forearc. Samples from Nemegt Uul exhibit calc-alkaline, LREE-enriched island arc as well as tholeiitic LREE-depleted backarc-basin signatures of predominantly juvenile composition (initial ε_{Nd}-values +6 to +10). We suggest that Nemegt Uul belongs to the Gurvan Sayhan and Zoolen island arc terrane rather than an accretionary prism, as previously proposed. Samples from Bayanleg-Hatuu and Tseel reveal LREE-enriched calc-alkaline arc as well as tholeiitic LREE-depleted to slightly enriched backarc-basin signatures. The remarkably wide range of initial ε_{Nd}-values of ca. +8 to −6 indicates juvenile as well as old crustal material with mean residence times up to 1.5 Ga. Nd isotopic data for Bayanleg-Hatuu and Tseel suggest a variably rejuvenated margin of a Paleoproterozoic microcontinent with an associated backarc basin. Our Nd-isotopic data for the CAOB in southern Mongolia indicate a highly heterogeneous composition, and we conclude that a juvenile arc-backarc segment in the eastern study area was juxtaposed with a rejuvenated Paleoproterozoic microcontinent.
© 2005 Elsevier B.V. All rights reserved.

Keywords: Central Asian Orogenic Belt; Mongolia; Neodymium isotopes; Geochemistry; Trace elements; Terrane analysis

* Corresponding author. Fax: +49 89 2180 4176.
E-mail address: christoph.helo@gmx.de (C. Helo).

0009-2541/$ - see front matter © 2005 Elsevier B.V. All rights reserved.
doi:10.1016/j.chemgeo.2005.10.003

1. Introduction

The Central Asian Orogenic Belt (CAOB) represents a segment of largely juvenile continental crust that formed from the Neoproterozoic to the late Mesozoic by accretion of island arcs and subordinate early to mid-Precambrian microcontinents (Sengör et al., 1993; Mossakovsky et al., 1994; Badarch et al., 2002; Filippova et al., 2001; Yakubchuk, 2002; Khain et al., 2003; Kheraskova et al., 2003; summary of further references in Jahn et al., 2000a, 2004a). Understanding of the details of the development of the CAOB has considerably progressed in recent years due to systematic geochronological and geochemical isotopic studies (Jahn et al., 2000b, 2004b; Wu et al., 2000, 2002; Buchan et al., 2002; Pfänder et al., 2002; Khain et al., 2002, 2003; Jahn, 2004; Kovalenko et al., 2004; Kuzmichev et al., 2005). In Mongolia the well-exposed central part of the CAOB offers an exceptional opportunity to study the orogen from its inception in the Neoproterozoic (as pointed out by Khain et al., 2002, the inception was in the Mesoproterozoic at least 1020 Ma ago) to its culmination in the late Permian. Using structural, geological, metamorphic, and paleontological data, Badarch et al. (2002) presented a synthesis of the CAOB in Mongolia in the form of a multiple terrane model. For a better understanding of the history of the CAOB this model needs to be tested and augmented with new geochronological and geochemical isotopic data.

We present a reconnaissance geochemical and Nd-isotopic study of ca. 470–290 Ma old metaigneous and metasedimentary rocks from southern Mongolia and provide the first comprehensive geochemical-Nd isotopic data set for an area extending from the Gurvan Sayhan range, west of the town of Dalanzadgad to Bayanleg-Hatuu, and the Tseel Mountain range (Fig. 1). The sampled localities belong to four terranes interpreted by Badarch et al. (2002) as an island arc, an accretionary prism complex, backarc-forearc basins, and a polymetamorphic block (Fig. 1a). The aim of this study was to elucidate the genesis of the rocks, constrain their tectonic setting, test the previously proposed terrane model, and explore the late-stage development of the southern CAOB.

2. Geological background

2.1. Overview of the Central Asian Orogenic Belt

The Central Asian Orogenic Belt (Fig. 1b) extends from the Urals, through Kazakhstan, northern China, Mongolia, and southern Siberia to the Okhotsk Sea in

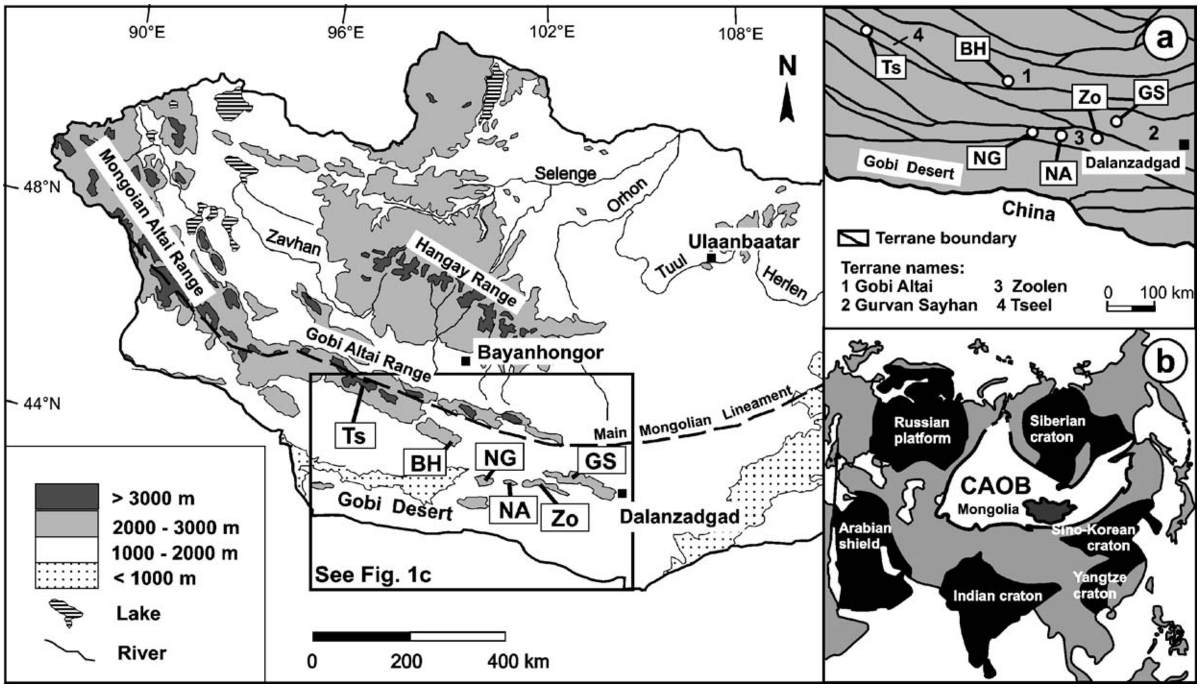

Fig. 1. Geographic map of Mongolia showing the study areas in the south. Inset (a) depicts the location of study areas and respective terranes of Badarch et al. (2002). Inset (b) depicts the Central Asian Orogenic Belt (CAOB) and surrounding cratons. Abbreviations: GS = Gurvan Sayhan (island arc terrane), Zo = Zoolen (accretionary prism terrane), NG = Nemegt Uul–Gilbent, NA = Nemegt Uul–Altan Uul (accretionary prism terrane), BH = Bayanleg-Hatuu (Gobi Altai backarc–forearc basin terrane), Ts = Tseel (Tseel polymetamorphic block).

the east of Russia (Sengör et al., 1993; Yakubchuk, 2002). It is sandwiched between the Siberian craton in the north and the Sino-Korean and Tarim cratons in the south. Sengör et al. (1993) proposed a speculative model involving oceanward growth of a single and laterally extensive island arc (Kipchak arc) and subsequent juxtaposition of arc segments by strike-slip stacking. More recently, alternative models were proposed that involved closure of small ocean basins along multiple subbduction zones, accretion of island arcs, and obduction of ophiolites (e.g. Mossakovsky et al., 1994; Badarch et al., 2002; Khain et al., 2003; Kuzmichev et al., 2005). Irrespective of these models, there is a consensus that the assembly of the CAOB in the Paleozoic to Mesozoic produced major growth of the continental crust (Sengör et al., 1993).

In Mongolia the CAOB may be subdivided into northern and southern domains, separated by a tectonic boundary along the Main Mongolian Lineament (Windley et al., 2004; see Fig. 1). The northern domain, previously termed Caledonian, consists of Neoproterozoic ophiolites, Precambrian and early Paleozoic metamorphic rocks, and early Paleozoic basins with clastic rocks, island arcs and associated volcaniclastic sediments. These are overlain by Devonian-Carboniferous sediments and crosscut by Permian-Triassic volcanic-intrusive rocks. The southern domain, formerly termed Hercynian, comprises mid to late Paleozoic island arcs, remnants of ophiolites, serpentinite mélanges, and upper Carboniferous to Permian volcanic rocks (see references in Badarch et al., 2002). Both domains were intruded by post-orogenic granites and are overlain by Jurassic-Cretaceous terrigenous volcanic and sedimentary rocks.

In their terrane model Badarch et al. (2002) defined 44 geologically distinct, fault-bounded lithotectonic terranes in Mongolia. They distinguished between island arcs, Andean-type continental margins, ophiolites, accretionary prisms, passive continental margins, older microcontinents, and lithogical units of unknown origin. The accretionary history of this mosaic of terranes is still poorly understood, but it possibly occurred by multiple accretion of island arcs and Precambrian microcontinents and closure of ocean basins in an environment similar to the present-day SW Pacific (Xiao et al., 2003, 2004).

2.2. Geology of the study areas

The study areas are located in southern Mongolia and occur in an area extending ca. 400 km to the west of the town of Dalanzadgad (Fig. 1). They are situated in four terranes defined by Badarch et al. (2002, Fig. 1a): (1) the Gobi-Altai backarc-forearc basin, (2) the Gurvan Sayhan island arc, (3) the Zoolen accretionary prism, and (4) the low to high-grade Tseel block. Below we present a brief description of these terranes relevant for the purposes of this study.

2.2.1. The Gurvan Sayhan island arc terrane

This arc terrane occupies an area of ca. 800 km by 200 km (Fig. 1a). It comprises Ordovician-Silurian greenschist-facies sediments and volcaniclastic rocks, Silurian-Devonian island arc tholeiites and andesites (Lamb and Badarch, 1997, 2001) as well as middle Devonian to lower Carboniferous volcaniclastic rocks that contain conodont-bearing chert yielding a Frasnian age of 360 Ma (Zonenshain et al., 1975; Badarch, 1990). Imbricated thrust sheets, dismembered blocks, tectonic mélange, and high strain zones further characterize this terrane. During the final stage of the pre-accretionary development of this terrane, terrigenous sediments of middle Carboniferous were deposited. Post-accretionary rock assemblages include intermediate and felsic volcanic rocks, overlain by terrigenous sediments. Emplacement of post-tectonic granitoids occurred from the early Silurian to late Permian (Badarch et al. 2002).

2.2.2. The Zoolen accretionary prism terrane

This terrane is ca. 500 km long and up to 80 km wide and juxtaposed with the Gurvan Sayhan island arc at its NE boundary (Figs. 1a and 2). It is made up of highly deformed rocks, metamorphosed under greenschist-facies conditions. Thrust sheets, tectonic slivers, and mélange contain Ordovician-Devonian pillow basalts and andesites (Lamb and Badarch, 2001). The volcanic rocks are associated with clastic sediments, limestones, and lower Carboniferous marine sediments and contain abundant fragments of mylonitized peridotite, serpentinite, and gabbro. Post-accretionary units are similar to those in the Gurvan Sayhan island arc and comprise volcanic and sedimentary rocks (Badarch et al., 2002).

2.2.3. The Gobi Altai backarc–forearc basin terrane

This terrane is ca. 1600 km long and up to 100 km wide (Fig. 1a). It is situated along the Main Mongolian Lineament, forming the northern margin of the southern Mongolian domain (Ruzhentsev, 2001; Badarch et al., 2002). The oldest rocks comprise Cambrian greenschist-facies volcaniclastic and subordinate volcanic rocks that are overlain by Ordovician-Silurian volcano-sedimentary units. The Cambrian-Silurian rocks

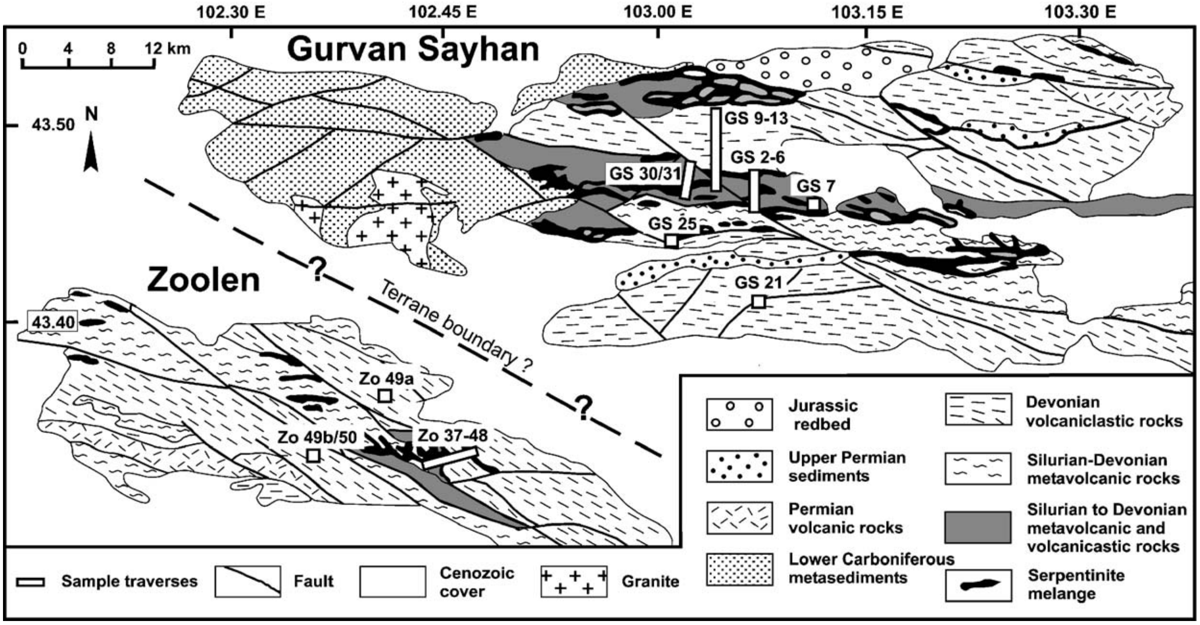

Fig. 2. Geological map (after Badarch, 1990) of the Gurvan Sayhan and Zoolen ranges with sample localities.

contain lenses of serpentinite and gabbro. The Devonian-Carboniferous conglomerates, sandstones, and siltstones are intercalated with pillow basalts, andesites, and tuffs. Granitoids of Silurian-Devonian and Carboniferous-Permian ages are abundant. Badarch et al. (2002) suggested that the thick sequences of volcaniclastic and subordinate volcanic rocks were deposited in backarc or forearc basins.

2.2.4. The Tseel polymetamorphic block

This NW-trending block is ca. 500 km long and up to 50 km wide (Fig. 1a) and represents the only locality in southern Mongolia exposing high-grade rocks (Kozakov et al., 2002; Badarch et al., 2002). In contrast to the Gurvan Sayhan, Zoolen and Gobi Altai terranes, it shows evidence for multiple metamorphic events (Kozakov et al., 2002) encompassing amphibolite (possibly granulite-facies)- to greenschist-facies metamorphism. The predominant rocks are tonalitic gneisses, amphibolites, mica schists, and syntectonic granitoids. Kozakov et al. (2002) interpreted concordant U–Pb zircon ages of 385 Ma and 371 Ma as reflecting peak metamorphism.

3. Sample localities

We collected samples at six localities or traverses located in four terranes (Fig. 1). The localities are situated in (1) the Gurvan Sayhan mountain range (Figs. 1 and 2), an area situated in the western part of the Gurvan Sayhan island arc terrane ca. 100 km to the west of the town of Dalanzadgad (coordinates of sample localities are listed in the Appendix), (2) the Zoolen mountain range in the central part of the Zoolen accretionary prism terrane, (3) the Nemegt Uul ranges (Gilbent locality), and (4) the Nemegt Uul ranges (Altan Uul locality), both part of the Zoolen accretionary prism terrane, (5) Bayanleg in the Gobi Altai backarc–forearc basin terrane, and (6) the polymetamorphic Tseel block.

3.1. Sample descriptions and crystallization ages

From a collection of 80 samples we selected 46 for major element analysis. After evaluation of their major element characteristics a subset of 26 samples was chosen for ICP-MS trace element analysis, and 33 samples for determination of Sm–Nd isotopic compositions. The sample set for the Gurvan Sayhan and Zoolen localities represents the main lithologies comprising mafic, intermediate, and felsic volcanic rocks, intrusive, and volcaniclastic rocks. The sample set does not take into account the actual proportions of the rock types. Fieldwork showed that the areas contain a high proportion of intermediate to felsic rocks as in modern mature island arcs with subordinate mafic rocks. We interpret the volcaniclastic samples to represent a large-scale average composition of the exposed crust in their source areas. Of the samples collected in the western study areas we preferentially analyzed mafic and felsic rocks because they are suited to address the primary

Table 1
Major and trace element data for metaigneous and metasedimentary rocks from southwestern Mongolia

Locality	Gurvan Sayhan													Zoolen									
Sample	GS 2	GS 4	GS 5	GS 6	GS 7	GS 9	GS 11	GS 13	GS 21	GS 25	GS 30	GS 31	GS 36a	Zo 37	Zo 38	Zo 39	Zo 41	Zo 42	Zo 47	Zo 48	Zo 49a	Zo 49b	Zo 50
Rock type[a]	Meta-B.-thol. (pillow)	Meta-B.-trans	Meta-Di.-calc	Meta-G.-calc	Meta-G.-calc	Meta-Gd.-thol	Meta-Vc.-calc	Meta-H	Meta-Vc.-thol	Meta-Gb.-calc	Meta-A–thol. (pillow)	Meta-B.-thol. (pillow)	Chert	Meta-D.-calc	Meta-A.-calc	Meta-Vc.-calc	Meta-Vc.-thol	Meta-B.-thol	Meta-R.-calc	Meta-A.-calc	Meta-Vc.-calc.	Meta-B.-thol.	Meta-B.-trans.
Age (Ma)																421 ± 3	417 ± 2.2						
SiO_2	48.27	50.77	60.16	70.78	76.92	64.05	51.80	40.92	57.39	52.66	52.25	50.02	87.04	64.81	58.56	62.24	65.73	46.85	72.12	55.34	61.85	50.15	50.77
TiO_2	1.16	0.92	0.27	0.26	0.14	0.43	1.07	0.01	0.67	0.5	1.41	0.96	0.22	0.47	1.00	0.69	0.70	1.21	0.50	1.02	0.71	0.62	1.37
Al_2O_3	15.23	14.72	13.11	14.42	12.55	17.08	15.67	0.53	14.08	17.34	14.33	15.06	4.97	16.71	15.17	16.46	12.93	17.08	13.81	16.22	16.04	17.8	16.72
Fe_2O_3*	13.81	13.44	7.76	3.38	1.1	2.55	10.64	7.80	5.14	9.28	13.07	13.12	3.33	4.57	9.9	7.23	7.96	11.99	3.70	6.94	5.19	9.83	9.4
MnO	0.20	0.31	0.14	0.06	0.03	0.05	0.21	0.12	0.29	0.14	0.20	0.22	0.08	0.11	0.17	0.11	0.09	0.15	0.07	0.09	0.12	0.15	0.15
MgO	3.80	6.97	7.11	1.53	0.51	1.23	4.92	38.13	1.36	5.84	3.66	4.59	1.08	2.13	3.76	2.53	1.52	4.92	1.13	4.47	1.60	3.57	5.35
CaO	9.20	6.48	5.13	1.77	0.67	3.16	6.17	0.12	6.89	7.11	8.11	9.86	0.29	2.56	3.59	2.64	3.42	7.86	0.85	5.85	5.14	10.51	7.53
Na_2O	4.07	3.26	3.1	4.69	5.74	5.74	2.33	b.d.	1.85	3.78	2.86	2.86	0.61	5.84	3.6	4.28	4.06	2.88	5.48	6.30	3.20	2.8	4.16
K_2O	0.36	0.49	1.18	1.49	0.85	1.81	3.40	0.01	5.56	1.22	2.24	0.85	1.00	0.68	0.71	1.12	0.99	0.51	0.71	1.40	2.95	0.03	1.11
P_2O_5	0.28	0.11	0.06	0.07	0.03	0.16	0.36	b.d.	0.39	0.09	0.39	0.12	0.05	0.12	0.26	0.09	0.23	0.14	0.06	0.47	0.17	0.18	0.56
LOI	4.0	2.9	2.0	1.6	0.6	1.5	3.0	12.5	5.7	1.8	1.1	1.9	1.1	1.9	3.3	2.55	2.3	5.3	1.6	1.8	2.6	4.3	2.8
Total	100.4	100.4	100.0	100.1	99.1	99.8	99.6	100.8	99.3	99.8	99.6	99.5	99.7	99.9	100.0	100.0	99.9	99.0	100.0	99.9	99.6	100.0	99.9
Mg#[b]	42	58	71	54	55	56	55	93	41	62	42	48	–	55	50	48	33	52	45	63	45	49	60
FeO*/MgO	3.3	1.7	1.0	2.0	1.9	1.9	1.9	0.2	3.4	1.4	3.2	2.6	2.8	1.9	2.4	2.6	4.7	2.2	2.9	1.4	2.9	2.5	1.6
Sr	–	335	248	473	185	920	–	–	377	–	744	–	35.9	–	–	–	860	578	252	–	621	–	–
Ba	–	99.7	324	264	127	380	–	–	1400	–	491	–	81	–	–	–	183	112	214	–	1080	–	–
Hf	–	1.7	1.33	2.09	2.91	3.02	–	–	3.51	–	4.06	–	1.05	–	–	–	1.43	1.94	5.56	–	2.88	–	–
Zr	–	57.2	41.9	82.2	102	125	–	–	131	–	156	–	37	–	–	–	50	73	198	–	111	–	–
Ta	–	0.25	0.31	0.60	0.69	0.52	–	–	0.37	–	0.49	–	0.67	–	–	–	0.40	0.25	0.33	–	0.42	–	–
Nb	–	2.39	1.07	1.66	2.30	2.20	–	–	4.40	–	6.77	–	1.64	–	–	–	2.68	2.85	3.64	–	5.33	–	–
U	–	0.35	0.55	0.29	0.52	0.50	–	–	1.10	–	1.61	–	0.28	–	–	–	0.33	0.19	0.84	–	1.24	–	–
Th	–	0.68	1.88	1.16	2.58	1.91	–	–	3.48	–	4.11	–	1.41	–	–	–	0.88	0.56	2.07	–	4.03	–	–
Pb	–	1.82	1.85	2.59	3.15	6.31	–	–	8.58	–	4.22	–	7.83	–	–	–	4.14	3.59	3.82	–	9.05	–	–
Y	–	18.8	6.07	6.51	5.37	3.29	–	–	25.2	–	28.8	–	7.23	–	–	–	20.6	17.8	36.3	–	19.5	–	–
Cr	–	31	–	–	–	–	–	–	–	–	38	–	–	–	–	–	–	255	–	–	–	–	–
Ni	–	17	–	–	–	–	–	–	–	–	22	–	–	–	–	–	–	141	–	–	–	–	–
La	–	5.95	5.96	8.39	11.4	15.4	–	–	19.1	–	29.3	–	7.02	–	–	–	10.8	6.64	12.5	–	18.2	–	–
Ce	–	15.2	11.6	17.3	22.6	30.5	–	–	40.4	–	63.1	–	15.8	–	–	–	20.4	15.9	30.4	–	36.6	–	–
Pr	–	2.21	1.39	2.14	2.53	3.48	–	–	5.00	–	8.20	–	1.90	–	–	–	3.09	2.36	4.33	–	4.27	–	–
Nd	–	10.8	6.1	8.9	9.2	13.0	–	–	21.5	–	35.4	–	7.92	–	–	–	13.8	11.5	20.1	–	17.5	–	–
Sm	–	2.98	1.42	1.84	1.59	2.11	–	–	4.84	–	7.55	–	1.61	–	–	–	3.38	3.31	5.23	–	3.80	–	–
Eu	–	1.04	0.48	0.60	0.33	0.64	–	–	1.43	–	2.06	–	0.32	–	–	–	1.12	1.26	1.15	–	1.18	–	–
Gd	–	3.35	1.33	1.58	1.15	1.39	–	–	4.64	–	6.73	–	1.56	–	–	–	3.70	3.67	5.70	–	3.74	–	–
Tb	–	0.53	0.18	0.20	0.15	0.15	–	–	0.72	–	0.91	–	0.22	–	–	–	0.56	0.57	0.93	–	0.54	–	–
Dy	–	3.55	1.13	1.24	0.90	0.75	–	–	4.53	–	5.55	–	1.39	–	–	–	3.44	3.53	6.09	–	3.41	–	–
Ho	–	0.73	0.22	0.24	0.18	0.12	–	–	0.92	–	1.07	–	0.27	–	–	–	0.69	0.68	1.30	–	0.70	–	–
Er	–	2.20	0.69	0.74	0.55	0.31	–	–	2.80	–	3.10	–	0.83	–	–	–	2.04	1.96	4.13	–	2.07	–	–
Tm	–	0.30	0.10	0.11	0.08	0.04	–	–	0.40	–	0.41	–	0.12	–	–	–	0.27	0.26	0.60	–	0.29	–	–
Yb	–	2.04	0.71	0.77	0.66	0.27	–	–	2.79	–	2.92	–	0.79	–	–	–	1.77	1.73	4.30	–	2.07	–	–
Lu	–	0.30	0.11	0.12	0.10	0.04	–	–	0.41	–	0.44	–	0.11	–	–	–	0.26	0.25	0.67	–	0.32	–	–
Th/Nb	–	0.28	1.76	0.70	1.12	0.87	–	–	0.79	–	0.61	–	0.86	–	–	–	0.33	0.20	0.57	–	0.76	–	–

Fe_2O_3* and FeO*, total iron as Fe_2O_3 and FeO, respectively. Major elements and Ni and Cr were analysed by XRF, values in wt.%; b.d. = below detection. Incompatible trace elements were analysed by ICP-MS, all values in ppm.

[a] H = harzburgite, B = basalt, A = andesite, D = dacite, Rd. = Rhyodacite, R = rhyolite, Vc = volcaniclastite, Gb = gabbro, Di = Diorite, Gd = granodiorite, G = granite, Amph = amphibolite; thol. = tholeiitic, trans. = transitional tholeiitic-calc-alkaline, calc. = calc-alkaline. For high-grade metamorphic rocks, protolith is given in brackets.

[b] Mg# = 100 × molar $Mg^{2+}/(Mg^{2+}Fe^{2+})$.

Table 1 (*continued*)

Locality	Nemegt Uul–Gilbert							Nemegt Uul–Altan Uul		Bayanaleg Hatuu							Tseel							
Sample	NG 54	NG 56	NG 57	NG 63	NG 66	NG 67	NG 72	NA 75	NA 77	BH 78	BH 79	BH 80	BH 81	BH 82	BH 83	BH 85	Ts 86	Ts 87	Ts 89	Ts 90	Ts 91	Ts 92	Ts 111	Ts 113
Rock type[a]	Meta-R.-thol.	Meta-B.-calc.	Meta-A.-thol.	Meta-B.-calc.	Meta-G.-thol.	Meta-A.-calc. (dike)	Meta-Gd.-calc.	Meta-A.-calc.	Meta-B.-thol.	Meta-Gd.-calc.	Meta-R.-calc.	Meta-G.-thol.	Meta-G.-calc.	Meta-Gb.-thol.	Meta-H.	Meta-Vc.-calc.	Amph (A.)-thol.	Amph (B.)-thol.	Meta-Gd.-calc.	Meta-D.-calc.	Gneiss G.-calc.	Meta-A.-thol.	Gneiss (Gd.)-calc.	Gneiss (G.)-thol.
Age (Ma)						318.6 ± 3.0						425.5 ± 1.1	467.1 ± 3.2						289.2 ± 2.3		360.5 ± 1.1		396.3 ± 2.9	397.0 ± 3.2
SiO_2	74.62	51.82	54.69	51.49	72.78	61.00	65.68	59.62	50.78	63.32	69.88	73.98	72.93	49.13	42.77	73.13	56.57	47.68	59.71	64.02	68.23	58.08	66.47	75.56
TiO_2	0.3	0.50	1.61	0.69	0.39	0.49	0.48	0.71	2.12	0.7	0.3	0.21	0.41	1.06	0.03	0.50	1.85	1.89	0.97	0.76	0.45	0.91	0.67	0.24
Al_2O_3	13.03	13.23	16.3	14.81	12.88	17.16	15.76	17.1	12.75	16.54	16	13.07	13.24	17.35	1.67	13.58	15.5	15.45	16.23	13.82	15.22	18.87	15.51	12.4
Fe_2O_3*	3.89	8.59	8.78	9.99	3.15	6.03	4.48	6.24	14.00	4.64	1.9	1.98	2.40	8.64	7.74	3.18	14.24	12.04	5.58	6.36	3.56	6.03	4.83	1.49
MnO	0.03	0.15	0.15	0.15	0.06	0.13	0.09	0.12	0.15	0.09	0.03	0.06	0.06	0.15	0.15	0.04	0.69	0.17	0.09	0.11	0.07	0.07	0.07	0.07
MgO	0.48	11.06	3.31	7.98	0.43	2.23	1.82	2.39	6.65	2.36	0.78	0.18	0.8	7.86	36.94	0.90	2.13	7.7	3.57	4.00	1.14	1.73	1.63	0.38
CaO	0.53	6.90	5.33	10.25	2.84	5.61	3.79	3.9	7.22	3.71	2.92	0.96	1.27	9.49	0.03	0.52	5.39	9.42	5.08	3.58	4.07	4.37	4.29	0.74
Na_2O	7.07	3.30	4.48	1.65	4.33	4.14	4.43	3.73	3.77	3.58	5.04	3.92	3.50	3.49	b.d.	2.65	1.05	3.31	3.84	2.55	3.57	5.00	4.39	6.41
K_2O	0.1	0.88	2.38	1.16	1.18	1.33	1.29	2.14	0.11	2.34	1.81	4.12	3.87	0.26	0.01	3.2	1.21	0.69	2.95	1.61	1.93	2.75	1.33	0.66
P_2O_5	0.04	0.09	0.7	0.04	0.07	0.17	0.1	0.18	0.18	0.16	0.09	0.02	0.08	0.09	u.d.l.	0.08	0.68	0.23	0.32	0.17	0.1	0.42	0.14	0.04
LOI	0.3	3.1	1.7	2.6	1.8	1.7	2.1	3.7	2.4	2.5	1.3	0.6	1.3	2.7	11.3	2.1	0.2	1.12	1.16	2.73	0.9	1.01	0.78	1.19
Total	100.4	99.8	99.4	100.8	99.9	99.9	100.0	99.9	100.2	99.9	100.0	99.1	99.8	100.3	101.1	99.9	99.5	99.8	99.5	99.7	99.2	99.2	100.1	99.2
Mg#[b]	25	77	50	68	26	49	52	50	56	57	52	19	47	71	93	43	28	63	63	62	46	43	47	40
FeO*/MgO	7.3	0.7	2.4	1.1	6.6	2.4	2.2	2.3	1.9	1.8	2.2	9.9	2.7	1.0	0.2	3.2	6.0	1.4	1.4	1.4	2.8	3.1	2.7	3.5
Sr	–	170	–	–	111	–	–	664	73.4	505	–	75.2	–	297	–	–	181	294	1100	242	334	1250	397	364
Ba	–	281	–	–	189	–	–	642	6.01	558	–	609	–	96	–	–	91	58	884	333	492	1060	288	361
Hf	–	1.62	–	–	2.4	–	–	3.17	3.52	3.96	–	6.03	–	2.14	–	–	7.00	1.24	2.11	3.46	2.54	2.57	1.94	2.66
Zr	–	58	–	–	59	–	–	116	127	155	–	211	–	80	–	–	315	40	73	135	97	122	63	85
Ta	–	0.14	–	–	0.63	–	–	0.34	0.28	0.84	–	1.92	–	0.22	–	–	–	–	–	–	–	–	–	–
Nb	–	1.54	–	–	1.34	–	–	4.52	2.87	9.89	–	19.6	–	2.56	–	–	37.0	10.6	12.9	14.1	8.55	8.73	17.6	22.3
U	–	0.47	–	–	0.69	–	–	0.66	0.16	2.01	–	1.60	–	0.14	–	–	0.97	0.23	2.10	2.21	1.32	1.52	1.75	2.37
Th	–	0.78	–	–	0.43	–	–	2.76	0.15	8.03	–	14.5	–	0.26	–	–	3.58	0.83	16.2	10.9	13.1	2.34	8.25	10.4
Pb	–	2.60	–	–	2.92	–	–	4.80	0.55	15.7	–	18.3	–	6.53	–	–	7.44	3.34	22.3	32.1	9.40	14.6	4.01	4.03
Y	–	11.8	–	–	30.2	–	–	17.8	44.9	11.7	–	43.1	–	24.0	–	–	102	25.8	23.4	25.6	13.7	12.8	23.2	12.5
Cr	–	999	–	–	–	–	–	–	–	–	–	–	–	275	–	–	–	–	–	–	–	–	–	–
Ni	–	259	–	–	–	–	–	–	–	–	–	–	–	137	–	–	–	–	–	–	–	–	–	–
La	–	4.94	–	–	4.21	–	–	13.8	4	23.3	–	36.9	–		–	–								
Ce	–	11.3	–	–	11.7	–	–	30.0	13.2	47.2	–	77.4	–	3.54	–	–	39.0	10.2	63.1	27.5	52.2	16.1	30.9	41.3
Pr	–	1.56	–	–	1.95	–	–	3.86	2.33	5.06	–	8.94	–	10.0	–	–	94.1	23.9	128	59.3	101	30.9	71.0	72.9
Nd	–	7.31	–	–	10.2	–	–	16.6	13.1	18.4	–	34.1	–	1.61	–	–	13.2	3.34	14.8	7.0	10.6	3.94	7.81	7.28
Sm	–	1.89	–	–	3.29	–	–	3.77	4.76	3.28	–	7.10	–	8.69	–	–	59.9	15.4	56.2	27.0	35.8	16.8	29.8	23.2
Eu	–	0.60	–	–	0.78	–	–	1.19	1.62	0.95	–	1.01	–	2.89	–	–	15.6	4.04	8.89	5.48	5.26	3.41	5.56	3.22
Gd	–	2.02	–	–	4.20	–	–	3.53	6.69	2.64	–	7.02	–	1.04	–	–	5.23	1.42	2.17	1.33	1.29	1.48	1.32	0.74
Tb	–	0.32	–	–	0.75	–	–	0.55	1.16	0.37	–	1.17	–	3.82	–	–	17.8	4.70	6.33	4.94	3.82	3.10	4.90	2.33
Dy	–	2.09	–	–	5.19	–	–	3.33	8.02	2.19	–	7.58	–	0.64	–	–	3.02	0.77	0.83	0.81	0.50	0.43	0.69	0.36
Ho	–	0.43	–	–	1.10	–	–	0.67	1.70	0.42	–	1.55	–	4.33	–	–	19.2	4.90	4.66	4.85	2.69	2.46	4.33	2.18
Er	–	1.29	–	–	3.48	–	–	2.01	5.16	1.22	–	4.64	–	0.88	–	–	4.00	1.03	0.90	0.98	0.52	0.49	0.87	0.44
Tm	–	0.18	–	–	0.51	–	–	0.29	0.74	0.17	–	0.67	–	2.69	–	–	11.7	2.88	2.43	2.73	1.45	1.32	2.53	1.32
Yb	–	1.26	–	–	3.60	–	–	1.94	4.83	1.12	–	4.33	–	0.36	–	–	1.70	0.39	0.33	0.39	0.21	0.18	0.36	0.20
Lu	–	0.19	–	–	0.53	–	–	0.30	0.70	0.16	–	0.59	–	2.40	–	–	11.0	2.55	2.23	2.54	1.37	1.17	2.36	1.44
				–		–	–				–		–	0.34	–	–	1.64	0.37	0.34	0.39	0.22	0.18	0.36	0.24
Th/Nb	–	0.51	–	–	0.32	–	–	0.61	0.05	0.81	–	0.74	–	0.10	–	–	0.10	0.08	1.25	0.77	1.53	0.27	0.47	0.47

goals of this study which are to define the composition of mantle sources, infer geotectonic settings, and evaluate crustal growth and recycling of older crust. The subordinate intermediate rock types from these areas (in fact a remarkable feature of all these terrains is the small amount of andesite) were not analyzed because they are probably related to the mafic rocks by crystal fractionation and thus do not provide additional information.

The samples from the island arc, accretionary prism, and forearc–backarc terranes underwent greenschist-facies metamorphism and those from the Tseel block mainly amphibolite- and greenschist-facies metamorphism.

Mineral assemblages of epidote-chlotite-amphibole, typical for greenschist-facies metamorphism, characterize the rock samples of mafic to intermediate compositions from the low-grade assemblages. The mafic metavolcanic rocks reveal a former glassy matrix with clinopyroxene now altered to fine-grained chlorite. In a few cases alteration of the matrix produced hematite. Phenocrysts of plagioclase are partially altered to fine-grained white mica and calcite, whereas olivine is completely replaced by spherical aggregates of fibrous serpentine. Clinopyroxene phenocrysts are mostly preserved without alteration. Coarse-grained secondary calcite can be observed in some samples.

The metavoclanic rocks of intermediate composition reveal a former matrix of glass altered to fine-grained chlorite. Plagioclase laths are partially altered to contain fine-grained white mica and calcite. Alteration of brown-greenish hornblende to epidote as well as to chlorite is ubiquitous. Clinopyroxene is in many cases well preserved and in some samples it has been replaced by greenish hornblende. Alteration of clinopyroxene to epidote and chlorite can also be observed. The samples show abundant quartz.

The metavolcanic rocks of felsic composition reveal a large proportion of fine-grained quartz, often exhibiting recrystallization structures. An equigranular texture and equilibrated grain boundaries are common. Coarse-grained alkalifeldspar and minor plagioclase show alteration to fine-grained assemblages of white mica. Perthitic strings and in some cases flameperthitic structures are present in alkalifeldspar. Muscovite is mostly fine- to medium-grained, and in a few cases preserved as coarse-grained flakes. The coarse mica flakes show sieve structures and fringed rims comprising epidote/clinozoisite, and chlorite. The samples typically reveal secondary epidote/clinozoisite crystals.

The granitic gneisses of the high-grade assemblages reveal coarse-grained mineral assemblages of quartz, alkalifeldspar, plagioclase, and biotite. Quartz exhibits distinct ductile deformation structures, such as bulging grain boundaries, and subgrainboundaries. Alkalifeldspat exhibits microcline twinning, perthitic strings as well as flameperthite, when in contact with plagioclase. Plagioclase exhibits polysynthetic twinning. Brown-greenish biotite occurs as oriented and isolated grains producing foliation. Metavolcanic biotite-quartz-schists exhibit fine-grained equigranular quartz as well as abundant medium to fine-grained biotite with frayed rims and a crenulation cleavage.

The age of the volcano-sedimentary sequences was determined on nine samples using U–Pb SHRIMP single zircon dating and the Pb–Pb evaporation method (Table 1). In addition paleontological data provided independent age constraints. Zircons in two samples from the Zoolen locality yielded mean ^{206}Pb–^{238}U SHRIMP ages of 421 ± 3.0 Ma (sample Zo 39) and 417 ± 2.2 Ma (sample Zo 41). Evaporation of zircons from two samples of the Bayanleg locality yielded 425.5 ± 1.1 Ma (sample BH 80) and 433.5 ± 1.1 Ma (sample BH 81). These ages are consistent with the paleontological evidence for a Silurian to early Devonian age of deposition (Eenzhin, 1983; Ruzhentsev et al., 1985) of the Gurvan Sayhan and Zoolen rock assemblages. We therefore accept an age of 420 Ma for calculation of initial Nd isotopic ratios for the samples from the Gurvan Sayhan, Zoolen, Nemegt Uul, and Bayanleg localities. Granitoid gneisses from the Tseel block yielded a ^{207}Pb–^{206}Pb zircon evaporation age of 360.5 ± 1.1 Ma, in agreement with a U–Pb zircon age of 357 Ma for a metagranitoid sample from the Tsogt block somewhat the east of the Tseel block (Kozakov et al., 2002). Further SHRIMP dating of zircons from the Tseel block yielded 397.0 ± 3.2 Ma, 396.3 ± 2.9 Ma, and 289.2 ± 2.3 Ma (Table 1). For the remaining samples from the Tseel block we assume an age of 360 Ma for calculation of initial ε_{Nd}-values.

4. Sample alteration and modification of the primary chemical composition

Most samples underwent greenschist-facies metamorphism, and those from the Tseel terrane amphibolite- to greenschist-facies metamorphism. Before interpreting the trace element data we need to address possible modification of the primary chemical composition of the samples due to alteration. Studies of low-temperature sample alteration have shown secondary enrichment of the large ion lithophile elements (LILE, e.g. Na, K, Rb, Cs), and U under oxidizing conditions, as well as enrichment in H_2O (e.g., Hart and Staudigel, 1989; Bach et al., 2001). In a study of fresh and altered basalt sample pairs from a core of oceanic crust, Bach et al. (2001) observed that Th, Ba, Sr, and Pb were modified only marginally. Seyfried et al. (1998), using hydrothermal sample alteration experiments, documented a high mobility of Rb and Cs and a restricted mobility for the alkaline earths Sr and Ba. In view of these findings we did not include the alkali metals and U in our interpretation of the data. As the primary concentrations of Ba, Sr, and Pb are possibly little altered, we interpreted their abundances as qualitative information on genetic processes. We placed most confidence in those elements known to behave immobile during weathering and metamorphic processes; these are the REE and the high-field strength elements (HFSE, Nb, Zr, Ti, Th; e.g. Pearce and Cann, 1973; Winchester and Floyd, 1976; Bailey, 1981; Pearce et al., 1984; Münker et al., 2004). We are positive that the Sm–Nd isotopic system was not disturbed in the samples that only underwent greenschist-facies metamorphism. For samples from the Tseel block with amphibolite-grade metamorphic overprinting, a modification of the Sm/Nd ratio cannot be precluded. On the other hand, the Sm/Nd ratios in the metagranitoids are not significantly different from typical crustal values (e.g. Fig. 4i) and indistinguishable from the values in rocks of similar composition that underwent only low-grade metamorphism. This agreement suggests that the Sm/Nd ratios in the high-grade samples from the Tseel block may be primary or only little modified.

5. Results

5.1. Major element data

The FeO*/MgO vs. SiO_2 classification diagram reveals calc-alkaline and tholeiitic rock compositions (Fig. 3; the analytical methods are listed in the Appendix). Besides predominantly calc-alkaline compositions, tholeiites are abundant among the metabasalts and basaltic metaandesites. Calc-alkaline rocks are typical constituents of mature island arcs, whereas tholeiitic rocks may be associated with emerging island arcs (e.g. Kuno, 1966; Miyashiro, 1974) as well as mid-ocean ridges, and backarc-basin spreading centers (e.g. Gill, 1976). Most of the basaltic samples have low TiO_2-concentrations of ca. 0.5–1.3 wt.% (Table 1), similar to igneous rocks from magmatic arcs (Pearce and Cann, 1973). High TiO_2-concentrations as in basalts from intra-plate settings were measured in two metabasalt samples from the Bayanleg and Tseel localities (Table 1). These samples are tholeiites and exhibit REE patterns similar to those in basalts from oceanic ridges. The Mg-numbers for all

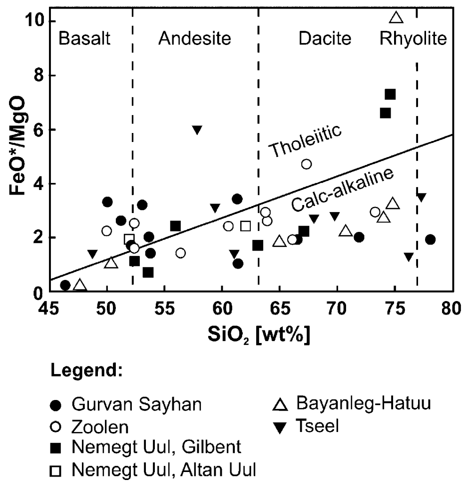

Fig. 3. SiO_2 versus FeO*/MgO classification diagram for igneous rocks from South Mongolia (modified after Miyashiro, 1974). The data were recalculated to anhydrous compositions to facilitate comparison of the samples.

samples range from about 20 in felsic rocks to 90 in a metadunite with cumulate olivine. A number of basalt samples have Mg-numbers of ca. 70, indicating near-primary mantle-derived compositions. Most andesitic samples are moderately fractionated with Mg-numbers of 50–60. Remarkable is metadiorite sample GS 5 with high MgO (7.1 wt.%) and a SiO_2 concentration (60 wt.%) that is similar to high-Mg andesites from forearcs (e.g., Hickey and Frey, 1982). A chert sample with high Al_2O_3 (5 wt.%) and K_2O (1 wt.%) concentrations apparently contains a high proportion of terrigenous clay (see trace element data presented below). We suggest that the terrigenous material in the chert reflects the composition of pelagic sediment. The volcaniclastic samples, interpreted as large-scale averages of exposed island arc crust, have 57–66 wt.% SiO_2 in the Gurvan Sayhan and Zoolen terranes. A mean of 61 wt.% SiO_2 suggests a somewhat more evolved crust than in the Mariana island arc (55 wt.% SiO_2; Stern et al., 2003) and the Quaternary Japanese arc (57 wt.% SiO_2; Aramaki and Ui, 1982). A volcaniclastic sample from the Bayanleg locality in the Gobi-Altai terrane has 73 wt.% SiO_2 (Table 1), suggesting an overall felsic composition of the exposed deposits of the inferred forearc–backarc basin assemblages.

5.2. Rare earth and other incompatible trace element data

5.2.1. Gurvan Sayhan island arc terrane

The primitive mantle-normalized trace element patterns depict four rock suites with different magmatic histories (Fig. 4a,b; the analytical methods are listed in the Appendix). Calc-alkaline metaandesite GS 30 and metavolcaniclastic rock GS 21 show enrichments of LREE and fluid-soluble slab-derived elements such as Ba, U, Pb, and Sr relative to the LREE (Fig. 4a). The high-field strength elements (HFSE) Nb and Ti display negative concentration anomalies. All of these chemical characteristics support melting of a subduction-modified mantle comprising fluids and melts from a dehydrating slab (e.g., Kay, 1984; Münker et al., 2004). A melted sedimentary component (Johnson and Plank, 1999) in these samples is suggested by the high Th/Nb ratios of 0.6 (GS 30) to 0.8 (GS 21) when compared to a ratio of ca. 0.05 in basalts derived from the depleted asthenosphere (Hofmann, 1988). Furthermore, the low crustal-like Ce/Pb ratios of <10 support mantle sources that were overprinted by slab-derived components (Taylor and McLennan, 1985). The good agreement between the trace element patterns of the metaandesite and the metavolcaniclastic samples support our field observation that the Gurvan Sayhan range has a largely intermediate to felsic composition.

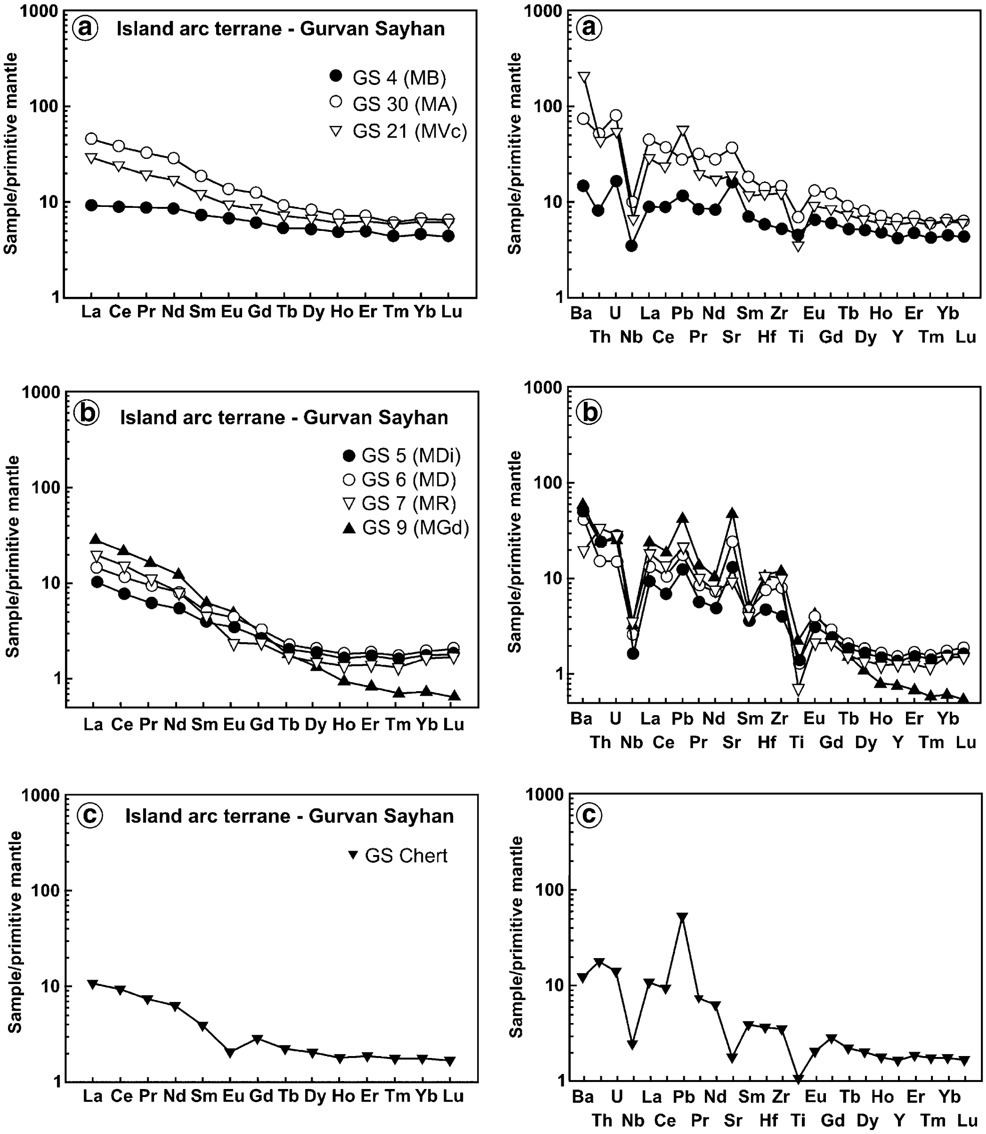

Fig. 4. REE and trace element patterns, normalized to primitive mantle values, of metaigneous and metavolcaniclastic sedimentary samples from southern Mongolia. Normalizing values from McDonough and Sun (1995); sequence of elements from Hofmann (1988). Abbreviations: M = meta-, B = basalt, A = andesite, D = dacite, Di = diorite, R = rhyolite, Gd = granodiorite, G = Granite, Gb = gabbro, Vc. = volcaniclastic rock, Amph = amphibolite.

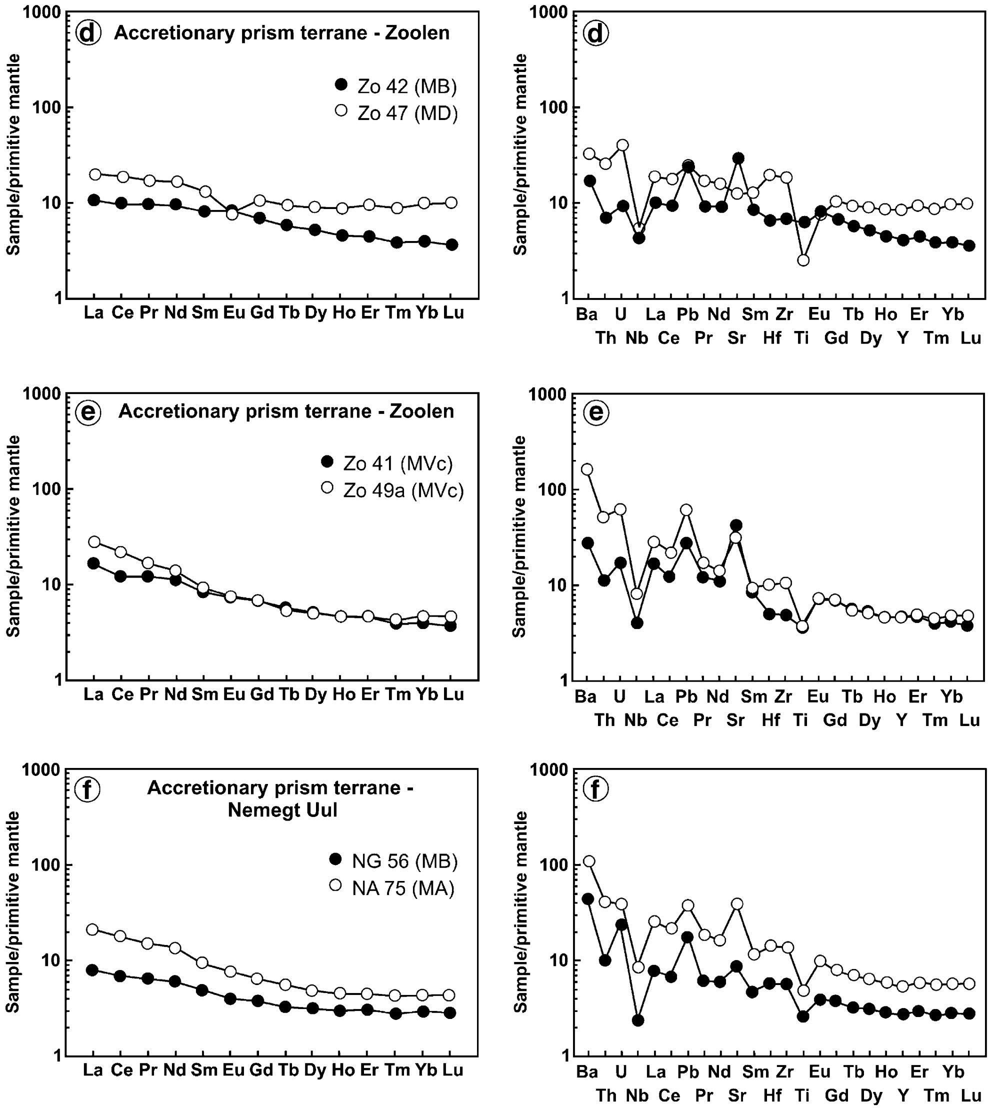

Fig. 4 (*continued*).

A second type of sample is represented by calc-alkaline metaandesite GS 5, metadacite GS 6, and metarhyolite GS 7 (Fig. 4b) all exhibiting distinctly fractionated REE patterns and low HREE abundances of ca. 2–3 times primitive mantle. The samples exhibit concave HREE patterns due to fractionation of hornblende, which plays an important role in thick and mature island arcs (e.g., Green, 1980; Kay and Gordillo, 1984). The LREE abundances increase with the degree of differentiation, e.g. the metarhyolite shows the highest enrichment in LREE, suggesting that these samples, collected in a restricted area, are probably related by crystal fractionation. Tholeiitic metabasalt GS 4 is different from the abovementioned samples (Fig. 4a) in that it exhibits little enrichment of LREE and the fluid-mobile elements Ba, U, Pb, and Sr. In agreement with the other samples it displays a negative Nb-anomaly. The trace element pattern and tholeiitic composition of the metabasalt are similar to those of basalts from incipient and immature island arcs (e.g. Kuno, 1966; Stern et al., 2003). A low Th/Nb ratio of 0.3 as well as little enrichment of the LREE suggests a very small amount of a recycled sedimentary component in this sample. Metagranodiorite sample GS 9 is distinct in that it has a chemical composition similar to that of adakitic rocks (Defant and Drummond, 1990). This can be seen in the strongly fractionated LREE/HREE pattern and fractionated HREE abundances, con-

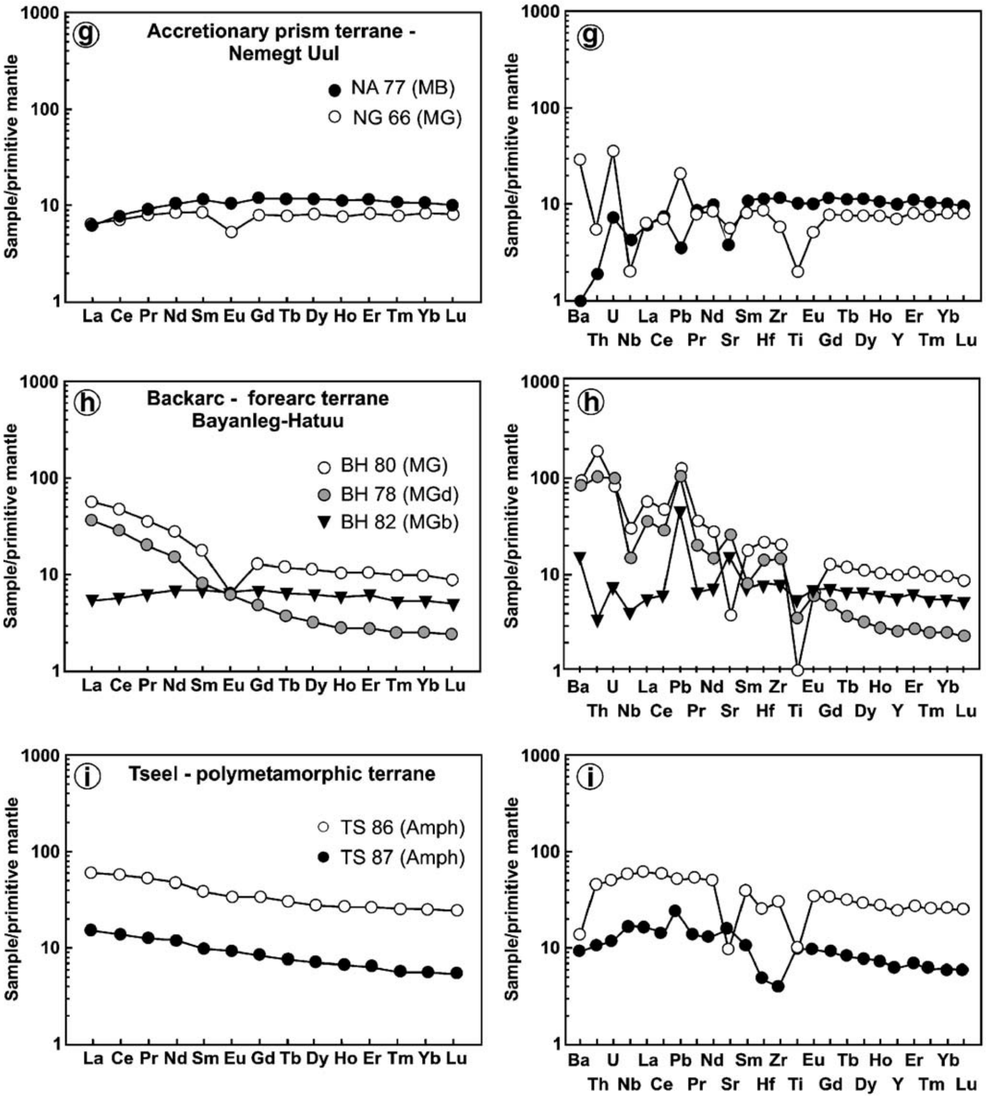

Fig. 4 (*continued*).

sistent with an eclogite source (e.g., Rapp et al., 1999). Furthermore, the sample exhibits distinct positive anomalies for fluid-mobile Ba, Pb, and Sr, and negative ones for immobile Nb and Ti. It has a high Al_2O_3 concentration of 17 wt.% and a very high Sr/Y ratio of 280. A high Th/Nb ratio of 0.9 and low Ce/Pb ratio of ca. 5 are consistent with a recycled sedimentary component in this sample. Yet, a high initial ε_{Nd} value of +8 in the sample requires that the recycled sediment was of juvenile composition. All of these chemical characteristics can be explained by melting of multiple sources including eclogitic oceanic crust, sediment, and a subduction-modified mantle wedge (Defant and Drummond, 1990). Metachert sample GS 36a (Fig. 4c) displays a trace element pattern as in shale representing average upper continental crust (Taylor and McLennan, 1985). Due to the high proportion of silica in the sample the REE concentrations are ca. three times lower than in upper crust-derived shale. A significant contribution of REE from seawater appears unlikely due to a lack of a negative Ce-anomaly (Murray, 1994; Kunimaru et al., 1998). The chert sample possibly represents pelagic sediment and its Nd isotopic composition may reflect the composition of subducted sediment.

5.2.2. The Zoolen accretionary prism terrane

The Zoolen locality is represented by a metabasalt and a metadacite sample (Fig. 4d) and two metavolcaniclastic samples (Fig. 4e). Tholeiitic metabasalt Zo 42

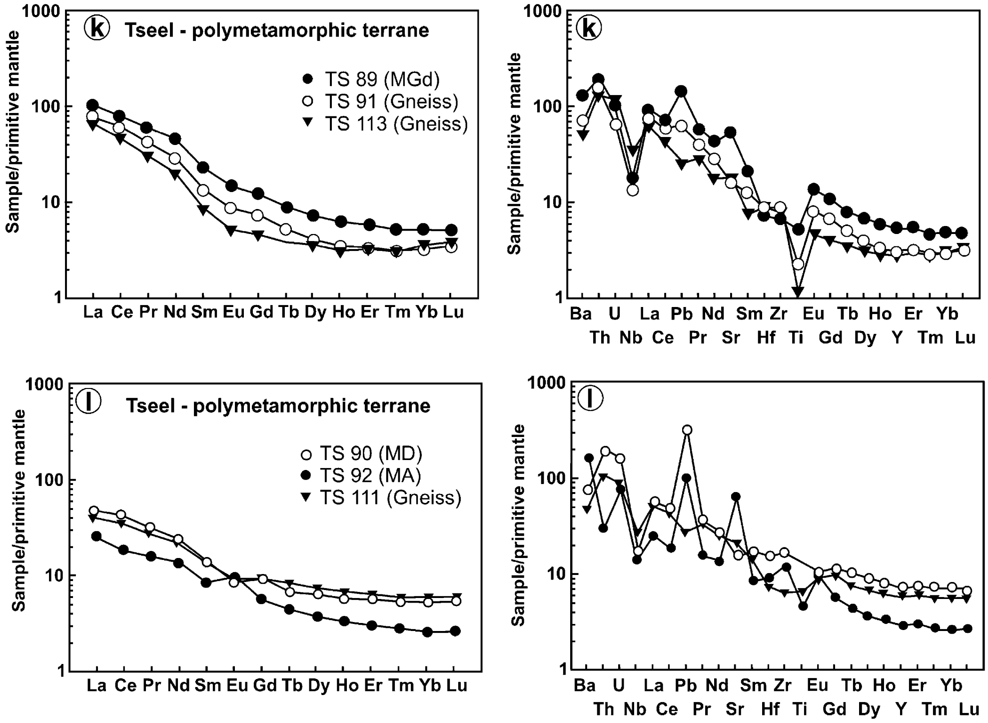

Fig. 4 (*continued*).

exhibits overall low concentrations of incompatible elements with little enrichment in the LREE. Subduction-related trace element characteristics such as positive anomalies for fluid-soluble Ba, Pb, and Sr, as well as a negative Nb-anomaly, are well developed. A low Th/Nb ratio of 0.3 is consistent with a small amount of recycled sediment in this sample. The sample is similar to tholeiitic metabasalt GS 4 from the Gurvan Sayhan range (Fig. 4a). The REE pattern of calc-alkaline metadacite Zo 47 is virtually unfractionated and displays negative Eu- and Ti-anomalies, indicating fractionation of plagioclase and Ti-magnetite. A slightly concave HREE pattern suggests additional fractionation of hornblende (Green, 1980). A high Th/Nb ratio of 0.5 and moderate abundances of Ba, U, and Pb confirm a slab-derived component in this sample. The metavolcaniclastite samples reveal moderate enrichment of the LREE and well-developed subduction-related trace element characteristics. A high Th/Nb ratio of 0.8 suggests a distinct amount of recycled sediment in sample Zo 49. A high initial ε_{Nd} value of +7.4 (Table 2) requires that the recycled components were of juvenile composition. The metavolcaniclastic sample Zo 41 has a moderately high Th/Nb ratio of 0.3 and accordingly lower LREE concentrations and fluid-soluble elements, except for Sr than sample Zo 49.

In the Nemegt Uul range (localities Gilbent and Altan Uul) we identified LREE-enriched calc-alkaline (metabasalt NG 56, metaandesite, NA 75) and LREE-depleted tholeiitic rocks (metabasalt NA 77, metaplagiogranite NG 66). The calc-alkaline samples show overall low REE concentrations, compatible with an origin from asthenosphere that had been depleted by removal of a MORB-melt (Ewart and Hawkesworth, 1987; Fig. 4f). High Th/Nb ratios of 0.5–0.6 are in agreement with the trace element evidence for a substantial slab-derived component in these samples. Tholeiitic metabasalt NA 77 and metaplagiogranite sample NG 66 display REE patterns as in moderately depleted mid-ocean ridge basalts (Fig. 4g). Negative concentration anomalies for Pb and Sr in combination with a very low Th/Nb ratio of 0.05 further support the MORB-like characteristics of the metabasalt. A positive U-anomaly may have been produced by U-uptake from seawater (Bach et al., 2001). In contrast, positive anomalies for Ba, U, Pb, and an elevated Th/Nb ratio of 0.3 in the metaplagiogranite sample indicate involvement of slab-derived components.

5.2.3. The Gobi Altai backarc–forearc basin terrane

The trace element patterns for a metagabbro, metagranodiorite, and metagranite sample from the Bayanleg-Hatuu locality are plotted in Fig. 4h. Tholeiitic

Table 2
Sm–Nd isotopic data for metaigneous and metasedimentary rocks from southwestern Mongolia

Sample	Rock type	Sm [ppm]	Nd [ppm]	$^{147}Sm/^{144}Nd$	$^{143}Nd/^{144}Nd(0)$	$\varepsilon_{Nd(t)}$	$T_{DM\ (Ga)}$
Gurvan Sayhan[a]							
GS 4 (420 Ma)	Metabasalt	3.00	10.8	0.1677	0.512909	6.8	*
GS 5 (420 Ma)	Metadiorit	1.38	5.92	0.1410	0.512870	7.5	*
GS 6 (420 Ma)	Metadacite	1.90	9.36	0.1229	0.512815	7.4	0.41
GS 7 (420 Ma)	Metarhyolite	1.58	9.25	0.1034	0.512752	7.2	0.42
GS 9 (420 Ma)	MetaGranodiorite	2.02	12.3	0.0992	0.512848	9.3	0.28
GS 21 (420 Ma)	Metavolcaniclast.	4.92	21.6	0.1375	0.512756	5.5	0.59
GS 30 (420 Ma)	Metaandesite	7.24	33.4	0.1311	0.512783	6.3	0.50
GS 36a (420 Ma)	Chert	1.68	8.04	0.1264	0.512585	2.7	0.80
Zoolen							
Zo 41 (417.0 ± 2.2 Ma)	Metavolcaniclast.	3.43	18.8	0.1103	0.512690	5.7	0.54
Zo 42 (420 Ma)	Metabasalt	3.32	11.7	0.1716	0.512937	7.2	*
Zo 47 (420 Ma)	Metadacite	5.27	20.2	0.1576	0.512891	7.0	*
Zo 49a (420 Ma)	Metavolcaniclast.	3.83	21.0	0.1101	0.512778	7.4	0.41
Nemegt Uul–Gilbent							
NG 56 (420 Ma)	Metabasalt	1.85	7.21	0.1553	0.512860	6.6	*
NG 66 (420 Ma)	Metaplagiogranite	3.27	10.1	0.1954	0.513113	9.3	*
Nemegt Uul, Altan Uul							
NA 75 (420 Ma)	Metaandesite	3.81	16.7	0.1377	0.512799	6.3	0.51
NA 77 (420 Ma)	Metabasalt	4.79	13.4	0.2164	0.513192	9.8	*
Bayanleg Hatuu							
BH 78 (420 Ma)	Metagranodiorite	3.38	19.0	0.1076	0.512542	2.9	0.73
BH 79 (420 Ma)	Metarhyolite	1.87	10.6	0.1067	0.512664	5.3	0.55
BH 80 (425.5 ± 1.1 Ma)	Metagranite	7.19	34.7	0.1253	0.512496	1.1	0.94
BH 81 (420 Ma)	Metagranite	5.59	29.0	0.1165	0.512509	1.8	0.84
BH 82 (420 Ma)	Metagabbro	2.97	9.2	0.1954	0.513019	7.5	*
BH 85 (420 Ma)	Metavolcaniclast.	6.12	31.69	0.1167	0.512333	−1.6	1.1
Tseel							
Ts 86 (360 Ma)	Amphibolite, andesitic	15.48	61.5	0.1522	0.512938	7.9	*
Ts 87 (360 Ma)	Amphibolite, basaltic	4.03	15.3	0.1596	0.512949	7.8	*
Ts 89 (289.2 ± 2.3 Ma)	Metagranodiorite	8.87	55.3	0.0969	0.512639	4.1	0.54
Ts 90 (360 Ma)	Metadacite	5.41	26.2	0.1246	0.512162	−6.0	1.4
Ts 90 repeat		5.12	24.8	0.1248	0.512152	−6.2	1.5
Ts 91(360.5 ± 1.1 Ma)	Gneiss, granitic	5.23	35.4	0.0892	0.512410	0.5	0.78
Ts 92 (360 Ma)	Metaandesite	3.52	16.6	0.1278	0.512750	5.4	0.54
Ts 94 (400 Ma)	Metavolcaniclast.	6.73	34.1	0.1191	0.512314	−2.4	1.2
Ts 95 (400 Ma)	Metaandesite	8.66	48.3	0.1083	0.512668	5.1	0.56
Ts 96 (400 Ma)	Felsic metatuffit	9.45	46.7	0.1225	0.512776	6.5	0.47
Ts 111 (396.3 ± 2.9 Ma)	Gneiss, granodioritic	5.61	28.7	0.1181	0.512638	4.0	0.66
Ts 113 (397.0 ± 3.2 Ma)	Gneiss, granitic	3.54	24.9	0.0860	0.512683	5.7	0.46

$^{143}Nd/^{144}Nd(0)$ = measured ratio, t = initial value. Within-run precision ($2\sigma_{mean}$) of $^{143}Nd/^{144}Nd \leq \pm 13$, except NG 66 = ± 15.
T_{DM} (depleted mantle model ages) were calculated according to DePaolo (1988).
*Sm/Nd too high for meaningful model age calculation.
[a] Ages in parentheses were used for calculation of initial ε_{Nd} values in cases where we have not determined a zircon age.

metagabbro BH 82 displays a MORB-like REE-pattern augmented with subduction-related characteristics for the fluid-mobile elements Ba, U, Pb, and Sr. It further displays a minute negative Nb-anomaly. This sample apparently contains fluid-mobile elements but lacks a substantial amount of a sedimentary component as is supported by a low Th/Nb ratio of 0.1. The metabasalt probably originated in a backarc basin-spreading center where subduction-related fluids were transported into the melting zone (e.g. Jenner et al., 1987; Bach et al., 1998; Taylor and Martinez, 2003). Calc-alkaline metagranodiorite BH 78 shows a fractionated REE pattern with low HREE abundances, and it lacks an Eu-anomaly. The REE pattern of metagranite sample BH 80 has a large negative Eu-anomaly and high abundances of HREE consistent with melting of plagioclase-bearing crustal sources.

5.2.4. The Tseel block

Tholeiitic metabasalt Ts 87 and metaandesite Ts 86 exhibit slightly enriched and subparallel REE-patterns (Fig. 4i). Similar ε_{Nd}-values of 7.8 and 7.9 in these samples support a comagmatic origin. Fractionation of olivine (see MgO concentrations in Table 1), and minor amounts of pyroxene and plagioclase as suggested by a negative Sr-anomaly and very weak Eu-anomaly (Eu/Eu* = 0.96), and magnetite, as reflected by a negative Ti-anomaly, may account for the trace element pattern in the andesite. Both samples are unusual in that they exhibit no trace element evidence for a slab-derived component (except for elevated Pb in the basalt). They also lack negative Nb-anomalies indicating an origin outside a subduction environment. The samples apparently originated in a ridge setting or at a seamount. The other group of samples comprises incompatible element enriched andesitic to granitic compositions (Fig. 4k, l) with concave REE patterns due to fractionation of hornblende (Fig. 4k). All of these samples show high concentrations of fluid-mobile elements and negative anomalies for Nb and Ti. Th/Nb ratios of 0.3–1.5 indicate substantial and in some cases high proportions of recycled sediment.

5.3. Sm–Nd isotopic data

The Sm–Nd isotopic data for 33 samples are listed in Table 2, and the initial ε_{Nd}-values are plotted in Fig. 5 (the analytical methods are listed in the Appendix). In Fig. 7 the initial ε_{Nd}-values are compared with published data for the CAOB. The initial ε_{Nd}-values for samples from Gurvan Sayhan, Zoolen, Nemegt Uul and Bayanleg-Hatuu are reported for an age of 420 Ma based on paleontological data, unless we have determined zircon ages for the samples. Initial ε_{Nd}-values of the samples from the Tseel block are reported for magmatic ages of 360 Ma and 400 Ma as inferred from paleontological evidence (Zonenshain et al., 1975), except for the samples for which we have determined zircon ages. An uncertainty in the age of the samples of ~40 Ma would not produce a significant error for the initial ε_{Nd}-value in samples with $^{147}Sm/^{144}Nd$ ratios >0.15 (e.g. for intermediate to mafic rocks). For LREE-enriched samples with low $^{147}Sm/^{144}Nd$ ratios of 0.1 to 0.12, an error of = 0.4 ε_{Nd}-units would be introduced. Thus, moderate uncertainties in the crystallization ages are not crucial for the interpretation of the data.

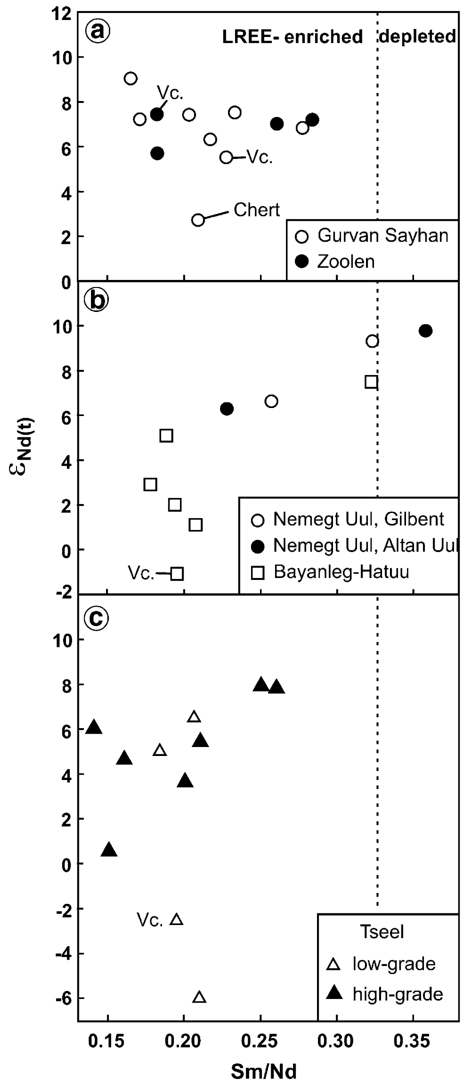

Fig. 5. Initial ε_{Nd}-values vs. Sm/Nd ratios for metaigneous rocks and metavolcaniclastic samples from South Mongolia. Vc.=metavolcaniclastic samples are interpreted as average composition of the exposed crust in the study areas.

In Fig. 5 the samples exhibit a very large spectrum of initial ε_{Nd}-values from ca. +10 to −6 with most samples displaying values of +10 to 0. Samples from the Gurvan Sayhan island arc and the Zoolen accretionary prism (Zoolen and Nemegt Uul localities) show high and similar initial ε_{Nd}-values of ca. +6 to +9 (Fig. 5). As Th/Nb ratios and LREE-patterns are consistent with variable proportions of recycled sediment in these samples, we adopt here an initial ε_{Nd}-value of ca. +10 as representing the depleted asthenosphere. Lower ε_{Nd}-values will be interpreted here, for the sake of simplicity, as due to recycling of older crustal material rather than melting of less depleted mantle sources. In this context the Nd isotopic data for the Zoolen and Nemegt Uul localities indicate crust with moderate to high proportions of juvenile material. A chert sample with a pelitic component yielding a low value initial ε_{Nd}-value of +2.7 suggests involvement of terrigenous material with an average crustal residence time of 0.8 Ga. The pelitic material in this sample represents a potential subduction component and may explain the isotopic heterogeneity in the intra-oceanic arcs that were formed remote from older continents, such as the Gurvan Sayhan island arc terrane. Initial ε_{Nd}-values of +5.5 to +7.4 in volcaniclastic samples from the Gurvan Sayhan and Zoolen ranges underscore a predominantly juvenile crustal composition of these terranes.

Samples from Nemegt Uul yielded initial ε_{Nd}-values similar to those from the Gurvan Sayhan and Zoolen Ranges. At this locality tholeiitic rocks, thought to have originated at a spreading ridge, have significantly higher initial ε_{Nd}-values of ca. +10 than the calc-alkaline samples with an average value of +6.5 (Fig. 5, Table 2). The difference in ε_{Nd}-values can be explained with recycling of an older sedimentary component in the arc-derived calc-alkaline rocks. This conclusion is supported by the their enrichment in the LREE and high Th/Nb ratios.

Involvement of large amounts of an older crustal component is evident in the granitoid and volcaniclastic samples from Bayanleg with initial ε_{Nd} values as low as −1.6. The recycled crustal material in these samples has a minimum average crustal residence time of 1.1 Ga. As the granitoids are partial melts of the basement, it is plausible to infer a variably rejuvenated old continental margin as their source. The fact that a volcaniclastic sample with an initial ε_{Nd}-value of −1.6 exhibits the largest proportion of old crustal material can be taken as strong evidence for erosion of an overall old crustal segment, much different from the Gurvan Sayhan and Zoolen ranges. In contrast to the in some cases low ε_{Nd}-values in the felsic samples, an associated LREE-depleted gabbro shows a high and mantle-like value of +7.5.

The high and low initial ε_{Nd}-values of +8 to −6 for samples from the Tseel block again demonstrate involvement of depleted mantle as well as old crustal sources. Samples from the high-grade portion of the Tseel block generally show a high proportion of juvenile mantle-derived material, whereas the low-grade units exhibits both juvenile and old crustal material with crustal residence ages up to 1.6 Ga (e.g sample Ts 90). We speculate that the high-grade rocks of the Tseel block as well as those from the Bayanleg localities represent a rejuvenated margin of an ancient microcontinent. The high-grade rocks may be interpreted as an uplifted arc root with a high proportion of underplated juvenile material, whereas the low-grade units may represent the upper crustal levels with a higher proportion of ancient crust.

6. Discussion

6.1. Analysis of tectonic components in the terranes

The inference of geodynamic settings for ancient rocks using geochemical criteria has a long tradition in geology (e.g., Pearce and Cann, 1973; Floyd and Winchester, 1975). Although many studies have produced controversial results, there is a consensus that tectonic discrimination diagrams provide meaningful results if the rocks under investigation were produced by modern-style plate tectonics. As the CAOB reveals typical elements of modern plate tectonics such as ophiolites and accretionary prisms, we are confident that a comparison of the geochemical characteristics with those in modern equivalents provides meaningful clues on the origin of the samples. Besides the robust REE and Nd-isotopes, we will explore elements that show a coherent behavior in samples from specific tectonic settings. For instance, in subduction-related igneous rocks the HFSE (e.g., Nb, Ta, and often Ti) show negative concentration anomalies relative to the neighboring REE, whereas the fluid-soluble elements (e.g., Ba, U, Sr, Pb) are enriched relative to the LREE. It can be assumed that the fluid-soluble elements were modified by hydrothermal sample alteration and metamorphism and that the primary concentrations are probably no longer preserved in the samples. On the other hand, as metamorphism is mostly of low-grade, we are positive that the primary pattern of these elements is preserved qualitatively. In addition, we interpret the fluid-immobile element Th (e.g., the Th/Nb ratio) as a proxy for melted and recycled sediment (Johnson and Plank, 1999).

In Fig. 6 the data are plotted in a tectonic discrimination diagram for mafic rocks. The basalts of this study are shown as solid symbols and more fractionated rock types as open symbols. The majority of samples has low Nb concentrations relative to La and Y and is therefore similar to island arc rocks. Most samples plot close to the La-apex and thus show an affinity to calc-alkaline island arcbasalts. Those samples plotting towards the Y-apex reveal an affinity with island arc tholeiites. We conclude that the calc-alkaline volcanic rocks represent thick and mature island arcs, whereas

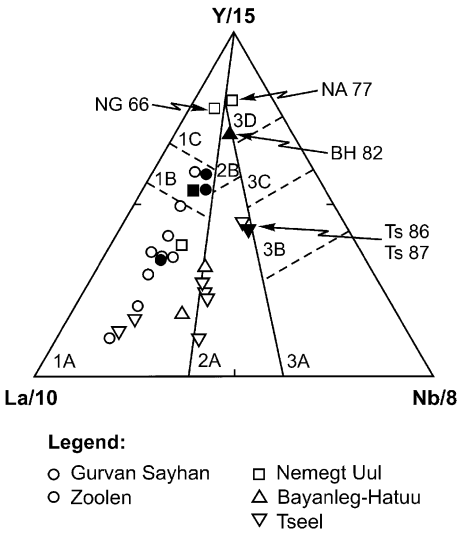

Fig. 6. Tectonic discrimination diagram based on immobile trace elements for metaigneous rocks from South Mongolia (after Cabanis and Lecolle, 1989; also in Rollinson, 1993). Explanation: 1A=calc-alkaline basalts, 1C=volcanic-arc tholeiites, 1B=overlap area between 1A and 1C; 2A=continental basalts, 2B=backarc-basin basalts; 3A=alkali basalts; 3B, C=enriched MORB; 3D=depleted MORB.

tholeiitic basalts immature arcs or backarc basins (e.g., Kuno, 1966; Miyashiro, 1974; Gill, 1976). A small number of samples plot in fields delineating enriched MORB (Ts 86 and 87), backarc basalts (BH 82), depleted MORB (NA 77), and arc tholeiites (NG 77). Some of the granitoid samples from the Tseel block plot in a field for alkali basalts, a result that is probably meaningless and may be due to their fractionated compositions. In the following we will place further constraints on the origin of the samples with the help of trace element patterns depicted in Fig. 4, Th/Nb ratios (Table 1), and Nd isotopes (Fig. 5; Table 2). As the CAOB in Mongolia predominantly comprises lithologies of intra-oceanic origin (Sengör et al., 1993; Badarch et al., 2002), a comparison with the intra-oceanic Izu-Bonin-Mariana island arc system (IBM) is useful to infer the tectonic setting. From the IBM a wealth of geochemical data and other information is available for forearc basins, magmatic fronts, and back-arc-basin assemblages (see overview by Stern et al., 2003).

6.1.1. Gurvan Sayhan island arc terrane

The Gurvan Sayhan range is made up of tholeiitic and calc-alkaline island arc rocks of predominantly intermediate composition. The calc-alkaline rocks exhibit strongly fractionated REE patterns due to amphibole fractionation that is important in thick and mature magmatic arcs (e.g., Kuno, 1966; Miyashiro, 1974). The tholeiitic samples may be assigned to an immature island arcs or magmatic front near a trench, or a back-arc-spreading center (e.g. Gill, 1976). A high-Mg metaandesite (sample GS 5) may be interpreted as a melt from depleted mantle peridotite overprinted by slab-derived components in the vicinity of a subducted mid-oceanic ridge (e.g., Deschamps and Lallemand, 2003). Furthermore, adakitic sample GS 9 suggests melting of subducted young and hot oceanic crust and portions of the mantle wedge (Defant and Drummond, 1990; Peacock et al., 1994). A typical setting for adakites and high-Mg andesites is a forearc. Finally, the abundant serpentinite in the study area (Fig. 2) may be interpreted as remnants of uplifted mantle in a tectonically unstable forearc (Stern et al., 2003). Regarding possible tectonic settings for the Gurvan Sayhan, Lamb and Badarch (2001) presented geochemical data for five samples and interpreted high concentrations of alkali metals in the carboniferous volcanic rocks as evidence for an alkaline composition and possibly a within-plate origin. Our large sample set does not support this conclusion. The robust Nb/Y ratio is <0.6 in all mafic samples, including the published data, and this is good evidence for a sub-alkaline composition (Pearce and Cann, 1973). In summary, the geochemical evidence and high initial ε_{Nd}-values for the Gurvan Sayhan range are consistent with an origin in a juvenile island arc-forearc setting.

6.1.2. Zoolen accretionary prism terrane

The igneous rocks from the Zoolen locality have tholeiitic and calc-alkaline compositions. Their trace element patterns and initial ε_{Nd}-values are similar to those in samples from the neighboring Gurvan Sayhan range. A similar composition of the Zoolen accretionary prism terrane and the Gurvan Sayhan island arc terrane is corroborated by the similarity in the trace element and Nd isotopic data of the volcaniclastic samples from both terranes (Figs. 4a,e and 5a). We interpret them as the composition of the exposed average island arc crust. Samples from Nemegt Uul also comprise calc-alkaline and tholeiitic rock varieties. An important finding is that tholeiitic metabasalt NA 77 displays all the features of depleted MORB (Fig. 4g). Metaplagiogranite NG 66 also reveals LREE-depletion as in MORB, yet an over-abundance of fluid-soluble elements that indicate a slab-derived component (Fig. 4g). The high initial ε_{Nd}-values of +9 to +10 in these samples indicate unusually depleted upper mantle sources different from those for the associated calc-alkaline samples with values of ca. +6.5. The LREE-depleted metabasalt and metaplagiogranite samples probably originated at a backarc-basin spreading center where LREE-depleted rocks with and without enrichment of fluid-mobile elements are ubiquitous (e.g., Gill, 1976; Jenner et al., 1987; Bach et al., 1998). The inferred island arc-backarc assemblages at Nemegt Uul may constitute part of the Gurvan Sayhan–Zoolen forearc–island arc or an unrelated transitional island arc–backarc segment. In any case, the evidence for a complex lithological make up of the Zoolen accretionary prism casts doubt on the previous notion of a single genetically coherent terrane.

6.1.3. Gobi Altai forearc-backarc basin terrane

At the Bayanleg locality ca. 100 km to the NW of Nemegt Uul, the samples may be assigned to a transitional magmatic arc (granitoid samples BH 78 and BH 80) and backarc basin (tholeiitic metagabbro BH 82). The trace element pattern of metagabbro BH 82 is consistent with an origin at a backarc-spreading ridge where incompatible element-depleted asthenosphere may be overprinted by fluids from a nearby subduction zone (e.g., Gill, 1976; Jenner et al., 1987, Bach et al., 1998). Contrasting the juvenile Gurvan Sayhan–Zoolen ranges, initial ε_{Nd}-values as low as -1.6 in the felsic and volcaniclastic samples indicate recycling of large amounts of older crustal material (Fig. 5b). The fact that the highest proportion of older crust ($T_{DM}=1.1$ Ga) is documented by a volcaniclastic sample suggests that the crust at the Bayanleg locality contains a high proportion of old material. We suggest that the Bayanleg locality is made up of remnants of a rejuvenated old microcontinent associated with a backarc basin, similar to a Japan-type magmatic arc.

6.1.4. The Tseel block

The volcanic and intrusive rocks from the high-grade segment of the Tseel block have predominantly calc-alkaline compositions with typical subduction-related trace element characteristics (Fig. 4j, k). Initial ε_{Nd}-values of $+5.4$ to $+0.5$ indicate juvenile and, in some samples, significant amounts of older crustal material. Mafic amphibolites (Fig. 4i) show somewhat enriched LREE patterns, high ε_{Nd}-values of $+8$, and they lack subduction-related trace element features. A possible tectonic setting for these samples is an oceanic ridge or seamount. An origin of these samples in a rifted arc is not plausible, because they show no evidence of slab-derived components. The initial ε_{Nd}-values of samples from the low-grade units of the Tseel block range from $+6.5$ to -6.0 and provide evidence for melting of juvenile as well as old crustal sources with residence times up to 1.5 Ga. The large range of initial ε_{Nd}-values in the samples may be explained with an origin in a magmatic arc situated on ancient continental crust, e.g. a microcontinent. In this context, the high-grade segment may represent the root of the inferred magmatic arc. Alternatively, low- and high-grade segments may have different origins and were juxtaposed during crustal amalgamation. In summary, the geochemical data for the Tseel block demonstrate a composite structure including remnants of a continental magmatic arc and oceanic crust (e.g. seamounts, oceanfloor). The evidence for ancient crust with average crustal residence times of ca. 1.5 Ga suggests a genetic relationship with the Bayanleg-Hatuu locality. An association of these localities with a Precambrian microcontinent is strongly favored.

6.2. Nd isotopic evidence for crustal recycling

A comparison of the initial ε_{Nd}-values with published data for the CAOB in Fig. 7 demonstrates two important findings about the composition and temporal development of the CAOB: (1) the island arc-ophiolite assemblages that formed between ca. 0.8 and 0.35 Ga are isotopically very heterogeneous and comprise juvenile crust as well as substantial amounts of recycled older crust, (b) during the final crustal accretion processes after ca. 0.3 Ga the production of juvenile mantle-derived material became subordinate and was replaced by processing of moderately juvenile and older crustal material. This shift in the isotopic composition of the crust may be due to closure of wide ocean basins and cessation of formation of island arcs remote from older cratons. In the final stage of orogenic development from ca. 300 to 200 Ma the Nd isotopes suggest that subduction zone magmatism had largely ceased and melting was relocated from the upper mantle to crustal levels with magmatic processing of sedimentary wedges, margins of microcontinents, and lower crustal blocks.

Although formation of juvenile crust is a striking feature of the of the CAOB (see Introduction for references), it is noteworthy that there is growing evidence that the orogen also comprises ancient crustal material (see special issues by Jahn et al., 2000a, 2004a; Wu et al., 2002; Pfänder et al., 2002; see summary of references in Kovalenko et al., 2004; Kuzmichev et al., 2005). This finding intuitively suggests a composite crustal structure with juvenile and interspersed ancient crustal blocks that were reworked during closure of ocean basins and the accretion of the juvenile island arcs.

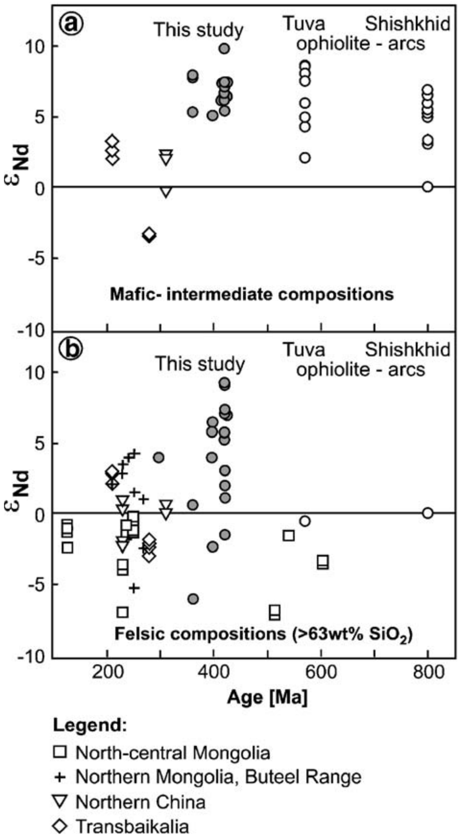

Fig. 7. Nd isotopic evolution diagram for metaigneous rocks and metavolcaniclastic samples from the CAOB. (a) Diagram showing data points for samples of mafic to intermediate composition, and b) samples of felsic composition. Data sources: Shishkhid ophiolite-island arc (Kuzmichev et al., 2005); Agardagh Ces-Tem (Tuva) ophiolite-island arc (Pfänder and Kröner, 2004); Buteel range (Hegner, unpubl. data); granitoids from north-central Mongolia (Jahn et al., 2004b); intrusive rocks from northern China (Chen et al., 2000); mafic-felsic volcanic and intrusive rocks from Transbaikalia (Litvinovsky et al., 2002).

The amount of recycled older crust in the CAOB is difficult to assess because the modeling needs to focus on a process that takes into account how older crustal material is recycled. Simple models involve mixing of melt batches derived from depleted mantle and older crust or melting of mixed sources comprising depleted mantle and a subducted sedimentary component. In order to explain a specific ε_{Nd}-value in a sample, a model involving mixing of discrete melt batches typically requires a ca. 10 times higher proportion of old crustal material than in the case of melting of a mixture of depleted mantle and subducted sediment. The difference in the calculated amount of a recycled older crustal material is due to the fact that a mantle-derived melt produced by ca. 10% of batch partial melting has a ca. 10 times higher Nd-concentration than the depleted mantle. In order to obtain meaningful estimates of the amount of recycled material, it is crucial to determine the process of how older crust is recycled. It is conceivable that in magmatic arcs built on older basement, MASH processes (melting, assimilation, storage, homogenization; Hildreth and Moorbath, 1988) and mixing of melt batches from older crust and mantle are important in addition to melting of mixed mantle sources. In island arcs situated on juvenile basaltic crust an old crustal component will probably be inherited from the mantle wedge with an added sedimentary component from the subducting slab. Using these scenarios as guidelines we calculate up to 6 wt.% of recycled old crustal material in the Gurvan Sayhan and Zoolen samples with initial ε_{Nd}-values of ca. +5. This estimate assumes melting of a mixed mantle source comprising a subducted sedimentary component with an ε_{Nd}-value of +2.7 inferred from metachert sample GS 36a. The calculation further assumes an initial ε_{Nd}-value of +10 and 1.3 ppm Nd in the depleted mantle. These values are suggested by MORB-like metabasalt NA 77 with an initial ε_{Nd}-value of +10 and 13 ppm Nd and assuming that it was produced by ca. 10% partial melting of the mantle. The accepted Nd concentration in the sedimentary component is 27 ppm as in average upper crust reported by Rudnick and Gao (2004). On the other hand, using a model of mixing melt batches, as probably relevant for the Tseel and Bayanleg samples where we suspect magmatic arcs on older basement, the amounts of recycled older crust would increase up to 30% to explain an ε_{Nd}-value of ca. 0. This estimate assumes melt batches from older crust with an ε_{Nd}-value of −6. Even though these estimates on recycling of older crust are rudimentary at best, the Nd isotopic data of the samples indicate a crustal mosaic comprising juvenile and ancient units and, by inference, a variety of tectonic settings including IBM-, Japan- or Andean-type continental margins.

7. Conclusions

(1) Geochemical and Nd isotopic data for igneous and volcaniclastic rocks of the CAOB in southern Mongolia indicate an origin in a juvenile island arc-backarc, and suggest juxtaposition of the arc with a rejuvenated margin of an ancient (>1.5 Ga) microcontinent.

(2) Analysis of the tectonic settings of the samples provides new information on the composition of the terranes delineated by Badarch et al. (2002). Our data show that the Gurvan Sayhan–Zoolen–Nemegt Uul

ranges comprise intraoceanic island arc-forearc–back-arc assemblages suggesting that they may represent segments of a common island arc. This interpretation is in conflict with the previous assignment of the Zoolen and Nemegt Uul ranges to an accretionary prism terrane. The data for samples from the Bayanleg-Hatuu locality within the Gobi-Altai forearc–back-arc basin terrane indicate an origin in a continental magmatic arc-backarc setting (Japan-like setting). The Tseel locality reveals similar geochemical characteristics as have been found at Bayanleg-Hatuu. We suggest that both localities are part of a rejuvenated margin of an ancient microcontinent.

Acknowledgements

We thank our colleagues from the Institute of Geology and Mineral Resources (IGMR), Mongolian Academy of Sciences, for their logistic support and efforts to get us to the field areas. Discussions with Alexander Rocholl and Wolfgang Schmidt helped to focus the content of the manuscript. The German Volkswagen-Foundation provided funding for field-work in Mongolia through a collaborative project between Mainz University and IGMR. E.H. thanks the German Research Foundation (DFG) for supporting the analytical work. Our sincere thanks go to B.-m. Jahn and the Editor R. Rudnick for their comments and recommendations to improve the manuscript. **[RR]**

Appendix A. Longitude and latitude positions of samples

Sample	Locality	Latitude	Longitude
GS 2	Gurvan Sayhan	43°47′ 06.1″	103°07′ 23.7″
GS 4	Gurvan Sayhan	43°46′ 56.2″	103°07′ 26.4″
GS 5	Gurvan Sayhan	43°46′ 56.2″	103°07′ 26.4″
GS 6	Gurvan Sayhan	43°46′ 56.2″	103°07′ 26.4″
GS 7	Gurvan Sayhan	43°46′ 13.7″	103°11′ 19.8″
GS 9	Gurvan Sayhan	43°47′ 41.4″	103°04′ 35.6″
GS 11	Gurvan Sayhan	43°48′ 17.5″	103°04′ 54.9″
GS 13	Gurvan Sayhan	43°51′ 27.3″	103°04′ 24.0″
GS 21	Gurvan Sayhan	43°41′ 59.9″	103°07′ 05.2″
GS 25	Gurvan Sayhan	43°44′ 08.1″	103°01′ 17.2″
GS 30	Gurvan Sayhan	43°47′ 36.3″	103°02′ 30.5″
GS 31	Gurvan Sayhan	43°47′ 48.8″	103°02′ 28.2″
GS 36a	Gurvan Sayhan	43°47′ 48.8″	103°02′ 28.2″
Zo 37	Zoolen	43°32′ 59.2″	102°44′ 55.6″
Zo 38	Zoolen	43°32′ 59.2″	102°44′ 55.6″
Zo 39	Zoolen	43°32′ 59.2″	102°44′ 55.6″
Zo 41	Zoolen	43°33′ 16.3″	102°45′ 49.4″
Zo 42	Zoolen	43°33′ 18.5″	102°45′ 48.6″
Zo 47	Zoolen	43°33′ 27.6″	102°46′ 50.7″
Zo 48	Zoolen	43°33′ 43.6″	102°46′ 58.2″
Zo 49a	Zoolen	43°36′ 02.7″	102°41′ 37.7″
Zo 49b	Zoolen	43°33′ 30.7″	102°36′ 19.1″
Zo 50	Zoolen	43°33′ 28.3″	102°36′ 12.3″
NG 54	Nemegt Uul, Gilbent	43°36′ 25.9″	101°32′ 48.0″
NG 56	Nemegt Uul, Gilbent	43°36′ 25.9″	101°32′ 48.0″
NG 57	Nemegt Uul, Gilbent	43°36′ 25.9″	101°32′ 48.0″
NG 63	Nemegt Uul, Gilbent	43°37′ 42.0″	101°34′ 31.5″
NG 66	Nemegt Uul, Gilbent	43°36′ 16.1″	101°34′ 04.9″
NG 67	Nemegt Uul, Gilbent	43°36′ 16.1″	101°34′ 04.9″
NG 72	Nemegt Uul, Gilbent	43°38′ 24.7″	100°40′ 29.5″
NA 75	Nemegt Uul–Altan Uul	43°41′ 05.9″	100°39′ 49.6″
NA 77	Nemegt Uul–Altan Uul	43°41′ 05.9″	100°39′ 49.6″
BH 78	Bayanleg-Hatuu	44°27′ 24.5″	100°47′ 02.8″
BH 79	Bayanleg-Hatuu	44°27′ 13.4″	100°46′ 52.9″
BH 80	Bayanleg-Hatuu	44°27′ 03.8″	100°46′ 42.5″
BH 81	Bayanleg-Hatuu	44°26′ 36.9″	100°45′ 47.6″
BH 82	Bayanleg-Hatuu	44°26′ 07.6″	100°44′ 58.3″
BH 83	Bayanleg-Hatuu	44°26′ 07.6″	100°44′ 58.3″
BH 85	Bayanleg-Hatuu	44°24′ 13.0″	100°43′ 09.6″
Ts 86	Tseel	45°02′ 16.8″	097°09′ 49.6″
Ts 87	Tseel	45°02′ 30.7″	097°10′ 23.6″
Ts 89	Tseel	45°02′ 11.7″	097°09′ 42.1″
Ts 90	Tseel	45°01′ 58.3″	097°09′ 20.1″
Ts 91	Tseel	45°04′ 11.2″	097°04′ 53.6″
Ts 92	Tseel	45°07′ 10.1″	097°06′ 56.2″
Ts 111	Tseel	45°26′ 51.1″	097°58′ 39.2″
Ts 113	Tseel	45°26′ 51.1″	097°58′ 39.2″

Appendix B. Sample preparation and analytical methods

The samples were crushed, and altered material was removed by handpicking before a rock powder was prepared in a tungsten-carbide mill. Tests of the extent of sample contamination with the carbide lining of the mill using quartz powder showed negligible contributions of Nb and Ta when compared with the concentrations in the samples. Major elements and Cr and Ni in mafic rocks were analyzed by X-ray fluorescence spectrometry (XRF) using a Philips PW 1404 with Rh-tube at the University of Mainz. The XRF–calibration curves were established with 56 international rock standards using the recommended values of Govindaraju (1989). Precision of SiO_2, TiO_2, Al_2O_3, Fe_2O_3, MgO, CaO is ≤0.2% (r.s.d.), that of Na_2O, K_2O, P_2O_5, Cr_2O_3, NiO ≤0.6% (r.s.d.), and that of MnO ≤0.9 (r.s.d.). The accuracy is estimated to be ca. 1% (r.s.d) for SiO_2 and Al_2O_3 and ca. 5% (r.s.d) for the other major elements.

Trace element concentrations and the REE were determined by ICP-MS at the GeoForschungsZentrum Potsdam using a Perkin-Elmer/SCIEX Elan 5000 mass spectrometer. Ca. 100 mg of sample powder was decomposed under pressure in a mixture of HF–$HClO_4$ in PTFE-bombs (DAS acid digestion system manufactured by Pico Trace, Germany) for about 16 h at 180 °C in order to accomplish dissolution of accessory phases. Details of the chemical procedures, instrumentation, data acquisition as well as typical values for procedure blanks, limits of detection, precision, and accuracy of the ICP-MS data are reported in Dulski (2001). A list of trace element determinations for 90 reference samples is supplied in the same publication. The limits of detection in rock samples were 2–8 ng/g for the REE, U, and Y, Sr (40 ng/g), Zr (116 ng/g), Ba (92 ng/g), Hf (45 ng/g), Pb (81 ng/g), Th (26 ng/g). The procedure blanks were generally below the limit of detection. For La and Ce procedure blanks of 20–50 ng/g were observed occasionally. The blank contributions are negligible for the samples under investigation. The precision of the analyses is generally ≤5% (r.s.d. for concentrations >1 μg/g), and the accuracy of the data ≤6% (r.s.d.) as inferred from well-known reference materials.

For Sm and Nd isotopic analyses the whole-rock powders were spiked with a ^{150}Nd–^{149}Sm tracer solution and dissolved in a mixture of HF–$HClO_4$ (Hegner et al., 1995a,b). All felsic and high-grade samples were decomposed in PTFE-bombs at 170 °C over 5 days, to ensure decomposition of accessory phases. The isotopic ratios were measured on a Finnigan MAT 261 mass spectrometer at the isotope laboratory of the Department of Earth and Environmental Sciences at the University of Munich using a dynamic quadruple mass collection mode for Nd and a dynamic single cup collection mode for Sm. Total procedure blanks for both elements are <60 pg and negligible for the samples of this study. The ^{143}Nd/^{144}Nd ratios were normalized to ^{146}Nd/^{144}Nd = 0.7219 and Sm isotopic ratios to ^{147}Sm/^{152}Sm = 0.51086. The long-term average for ^{143}Nd/^{144}Nd in our Ames metal Nd solution is 0.512141 ± 11 (2σ, N = 35) corresponding to 0.511853 in the La Jolla Nd-standard. The ^{147}Sm/^{144}Nd ratios in Table 2 are precise to 0.2% as verified with the CalTech-Sm/Nd standard solution.

References

Bach, W., Alt, J.C., Niu, Y., Humphris, S.E., Erzinger, J., Dick, H.J.B., 2001. The geochemical consequences of late-stage low-grade alteration of lower ocean crust at the SW Indian Ridge; results from ODP Hole 735B (Leg 176). Geochimica et Cosmochimica Acta 65, 3267–3287.

Bach, W., Hegner, E., Erzinger, J., 1998. Chemical fluxes in the Tonga subduction zone: evidence from the southern Lau Basin. Geophysical Research Letters 25, 1467–1470.

Badarch, G., 1990, Tectonics of the southern Mongolian foldbelts. Unpubl. doctoral thesis (in Russian), Uulaanbataar.

Badarch, G., Cunningham, W.D., Windley, B.F., 2002. A new subdivision for Mongolia: implications for Phanerozoic crustal growth in Central Asia. Journal of Asian Earth Sciences 21, 87–110.

Bailey, J.C., 1981. Geochemical criteria for a refined tectonic discrimination of orogenic andesites. Chemical Geology 32, 139–154.

Buchan, C., Pfänder, J., Kröner, A., Brewer, T.S., Tomurtogoo, O., Tomurhuu, D., Cunningham, D., Windley, B.F., 2002. Timing of accretion and collisional deformation in the Central Asian orogenic belt: implications of granite geochronology in the Bayanhongor ophiolite zone. Chemical Geology 192, 23–45.

Cabanis, B., Lecolle, M., 1989. Le diagramme La/10-Y/15-Nb/8: un outil pour la discrimination des series volcaniques et la mise en evidence des processus de melande et/ou de contamination crustale. Comptes Rendus de l'Académie des Sciences- Series II, vol. 309, pp. 2023–2029.

Chen, B., Jahn, B.-m., Wilde, S., Xu, B., 2000. Two contrasting Paleozoic magmatic belts in northern Inner Mongolia, China: petrogenesis and tectonic implications. Tectonophysics 328, 157–182.

Defant, M.J., Drummond, M.S., 1990. Derivation of some modern arc magmas by melting of young subducted lithosphere. Nature 347, 662–665.

Deschamps, A., Lallemand, S., 2003. Geodynamic setting of Izu-Bonin-Mariana boninites. Intra-Oceanic Subduction Systems: Tectonic and Magmatic Processes, Journal of the Geological Society of London, vol. 219. Special Publication, pp. 163–185.

Dulski, P., 2001. Reference materials for geochemical studies: new analytical data by ICP-MS and critical discussion of reference values. Geostandardands Newsletter 25, 87–125.

Eenzhin, G., 1983. The Southern Mongolian Hercynian Eugeocynaclinal Zone (Dzolen Range-Mandal-Ovoo) during Early Devonian time. Geotectonics 17, 326–334.

Ewart, A., Hawkesworth, C.J., 1987. The Pleistocene-Recent Tonga-Kermadec Arc lavas; interpretation of new isotopic and rare earth data in terms of a depleted mantle source model. Journal of Petrology 28, 495–530.

Filippova, I.B., Bush, V.A., Didenko, A.N., 2001. Middle Paleozoic subduction belts: the leading factor in the formation of the Central Asian fold-and-thrust belt. Russian Journal of Earth Sciences 3, 405–426.

Floyd, P.A., Winchester, J.A., 1975. Magma type and tectonic setting discrimination using immobile elements. Earth and Planetary Science Letters 27, 211–218.

Gill, J.B., 1976. Composition and age of Lau Basin and ridge volcanic rocks: implications for evolution of an interarc basin and remnant arc. Geological Society of America, Bulletin 87, 1384–1395.

Govindaraju, K., 1989. 1989 compilation of working values and sample descriptions for 272 geostandards. Geostandards Newsletter 13 (Special Issue), 113.

Green, T.H., 1980. Island arc and continental building magmatism—a review of petrogenetic models based on experimental petrology and geochemistry. Tectonophysics 63, 367–385.

Hart, S.R., Staudigel, H., 1989. Isotopic characterization and identification of recycled components, 1989. In: Hart, S.R., Gülen, L. (Eds.), Crust–mantle recycling in subduction zones. Cluver, Dordrecht, pp. 15–28.

Hegner, E., Roddick, J.C., Fortier, S.M., Hulbert, L., 1995a. Nd, Sr, Pb, Ar, and O isotopic systematics of Sturgeon Lake kimberlite, Saskatchewan, Canada: constraints on emplacement age, alteration, and source composition. Contributions to Mineralogy and Petrology 120, 212–222.

Hegner, E., Walter, H.J., Satir, M., 1995b. Pb–Sr–Nd isotopic composition and trace element geochemistry of megacrysts and melilitites from the Tertiary Urach volcanic field: source and composition of small volume melts under SW Germany. Contributions to Mineralogy and Petrology 122, 322–335.

Hickey, R.L., Frey, F.A., 1982. Geochemical characteristics of boninite series volcanics: implications for their source. Geochimica et Cosmochimica Acta 46, 2099–2115.

Hildreth, W., Moorbath, S., 1988. Crustal contributions to arc magmatism in the Andes of Central Chile. Contributions to Mineralogy and Petrology 98, 455–489.

Hofmann, A.W., 1988. Chemical differentiation of the Earth: the relationship between mantle, continental crust, and oceanic crust. Earth and Planetary Science Letters 90, 297–317.

Jahn, B.-m., 2004. The Central Asian Orogenic Belt and growth of the continental crust in the Phanerozoic. Geological Society Special Publications 226, 73–100.

Jahn, B.-m., Griffin, W.L., Windley, B.F. (Eds.), 2000a. Continental growth in the Phanerozoic; evidence from Central Asia, Tectonophysics, vol. 328, pp. 1–227.

Jahn, B.-m., Wu, F., Chen, B., 2000b. Massive granitoid generation in Central Asia; Nd isotope evidence and implication for continental growth in the Phanerozoic. Episodes 23, 82–92.

Jahn, B.-m., Windley, B.F., Natal'in, B., Dobretsov, N. (Eds.), 2004a. Phanerozoic Continental Growth in Central Asia, Journal of Asian Earth Sciences, vol. 23, pp. 599–815.

Jahn, B.-m., Capdevila, R., Liu, D., Vernon, A., Badarch, G., 2004b. Sources of Phanerozoic granitoids in the transect Bayanhongor–Ulaan Baatar, Mongolia: geochemical and Nd isotopic evidence, and implications for Phanerozioc crustal growth. Journal of Asian Earth Sciences 23, 629–653.

Jenner, G.A., Cawood, P.A., Rautenschlein, M., White, W.M., 1987. Composition of backarc basin volcanics, Valu Fa Ridge, Lau Basin: evidence for a slab-derived component in their mantle source. Journal of Volcanology and Hydrothermal Research 32, 209–222.

Johnson, M.C., Plank, T., 1999. Dehydration and melting experiments constrain the fate of subducted sediments. Geochemistry, Geophysics, Geosystems 1. doi:10.1029/1999GC000014.

Kay, R.W., 1984. Elemental abundances relevant for identification of magma sources. Philosophical Transactions of the Royal Society of London A, vol. 310, pp. 535–547.

Khain, E.V., Bibikova, E.V., Kröner, A., Zhuralev, D.Z., Sklyarov, E.V., Fedotova, A.A., Kravchenko-Berezhnov, I.R., 2002. The most ancient ophiolite of the Central Asian fold belt: U–Pb and Pb–Pb zircon ages for the Dunzhungur complex, Eastern Sayan, Siberia, and geodynamic implications. Earth and Planetary Science Letters 199, 311–325.

Khain, E.V., Bibikova, E.V., Salnikova, E.B., Kröner, A., Gibsher, A.S., Didenko, A.N., Degtyarov, K.E., Fedotova, A.A., 2003. The Palaeo-Asian ocean in the Neoproterozoic and early Palaeozoic: new geochronologic data and palaeotectonic reconstructions. Precambrian Research 122, 329–358.

Kheraskova, T.N., Didenko, A.N., Bush, V.A., Volozh, Yu.A., 2003. The Vendian-early Paleozoic history of the continental margin of eastern Paleogondwana, Paleoasian ocean, and Central Asian foldbelt. Russian Journal of Earth Sciences 5, 165–184.

Kozakov, I.K., Glebovitsky, V.A., Bibokova, E.V., Azimov, P.Ya., Kirnozova, T.I., 2002. Hercycnian granulites of Mongolian and Gobian Altai: geodynamic setting and formation conditions. Doklady Earth Sciences 38, 781–785.

Kovalenko, V.I., Yarmolyuk, V.V., Kovach, V.P., Kotov, A.B., Kozakov, I.K., Salnikova, E., Larin, A.M., 2004. Isotope provinces, mechanisms of generation and sources of the continental crust in the Central Asian mobile belt: geological and isotopic evidence. Journal of Asian Earth Sciences 23, 605–627.

Kunimaru, T., Shimizu, H., Takahashi, K., Yabuki, S., 1998. Differences in geochemical features between Permian and Triassic cherts from the Southern Chichibu terrane, southwest Japan: REE abundances, major element compositions and Sr isotopic ratios. Sedimentary Geology 119, 195–217.

Kuno, H., 1966. Lateral variation of basalt magma types across continental margins and island arcs. Bulletin of Volcanology 29, 195–222.

Kuzmichev, A., Kröner, A., Hegner, E., Liu, D., Wan, Y., 2005. The Shishkhid ophiolite, northern Mongolia: a key to the reconstruction of a Neoproterozoic island-arc system in central Asia. Precambrian Research 138, 125–150.

Lamb, M.A., Badarch, G., 1997. Paleozoic Sedimentary Basins and Volcanic-Arc Systems of Southern Mongolia: New Stratigraphic and Sedimentologic Constraints. International Geology Review 39, 542–576.

Lamb, M.A., Badarch, G., 2001. Paleozoic sedimentary basins and volcanic arc systems of southern Mongolia: new geochemical and petrographic constraints. In: Hendrix, M.S., David, G.A. (Eds.), Paleozoic and tectonic evolution of central Asia: From continental assembly to intracontinental deformation, Boulder, Colorado, Geological Society of America Memoir, vol. 194, pp. 117–149.

Litvinovsky, B.A., Jahn, B.-m., Zanvilevich, A.N., Saunders, A., Poulain, S., Kuzmin, D.V., Reichow, M.K., Titov, A.V., 2002. Petrogenesis of syenite-granite suites from Bryansky Complex (Transbaikalia, Russia): implications for the origin of A-type granitoid magmas. Chemical Geology 189, 105–133.

McDonough, W.M., Sun, S.S., 1995. The composition of the earth. Chemical Geology 120, 223–253.

Miyashiro, A., 1974. Volcanic rock series in island arcs and active continental margins. American Journal of Science 274, 321–355.

Mossakovsky, A.A., Ruzhentsev, S.V., Samygin, S.G., Kheraskova, T.N., 1994. Central Asian foldbelt: geodynamic evolution and formation history. Geotectonics 27, 445–474.

Münker, C., Wörner, G., Yogodzinski, G., Churikova, T., 2004. Behaviour of high field strengths elements in subduction zones: constraints from Kamchatka-Aleutian arc lavas. Earth and Planetary Science Letters 224, 275–293.

Murray, R.W., 1994. Chemical criteria to identify the depositional environments of chert: general principles and applications. Sedimentary Geology 90, 213–232.

Peacock, S.M., Rushmer, T., Thompson, A.B., 1994. Partial melting of subducted oceanic crust. Earth and Planetary Science Letters 121, 224–227.

Pearce, J.A., Cann, J.R., 1973. Tectonic setting of basic volcanic rocks determined using trace element analysis. Earth Planetary Science Letters 19, 290–300.

Pearce, J.A., Harris, N.B.W., Tindle, A.G., 1984. Trace element discrimination diagrams for the tectonic interpretation of granitic rocks. Journal of Petrology 25, 956–983.

Pfänder, J.A., Jochum, K.P., Kozakov, I., Kröner, A., Todt, W., 2002. Coupled evolution of back-arc and island arc-like mafic crust in the late-Neoproterozoic Agardagh Tes-Chem ophiolite, Central Asia: evidence from trace element and Sr–Nd–Pb isotopic data. Contributions to Mineralogy and Petrology 143, 1544–1574.

Pfänder, J.A., Kröner, A., 2004. Tectono-magmatic evolution, age and emplacement of the Agardagh Tes-Chem ophiolite in Tuva, Central Asia: crustal growth by island arc accretion. In: Kusky, T.M. (Ed.), Precambrian Ophiolites and Related Rocks. Elsevier, Amsterdam, pp. 207–221.

Rudnick, R., Gao, S., 2004. Composition of the Continental Crust. In: Rudnick, R.L. (Ed.), Treatise on Geochemistry, The Crust. Elsevier Pergamon.

Rapp, N., Shimizu, M.D., Applegate, G.S., 1999. Reaction between slab derived melts and peridotite in the mantle wedge: experimental constraints at 3.8 GPa. Chemical Geology 160, 335–356.

Rollinson, H., 1993. Using geochemical data: evaluation, presentation, interpretation. Prentice Hall, Longman Scientific and Technical, Harlow, United Kingdom (GBR). 352 pp.

Ruzhentsev, S.H., Badarch, H., Voznesenskaya, A., 1985. Tectonics of the Trans-Altai Zone of Mongolia (The Gurvansaykhan and Dzolen Ranges). Geotectonics 19, 276–284.

Ruzhentsev, S.V., 2001. The Variscan belt of South Mongolia and Dzungaria. In: Dergunov, A.B. (Ed.), Tectonics, Magmatism, and Metallogeny of Mongolia. Routledge, London, pp. 61–94.

Sengör, A.M.C., Natal'in, B.A., Burtman, S.V., 1993. Evolution of the Altaid tectonic collage and Palaeozoic crustal growth in Eurasia. Nature 364, 299–307.

Seyfried Jr., W.E., Chen, X., Chan, L.H., 1998. Trace element mobility and lithium exchange during hydrothermal alteration of seafloor weathered basalt; an experimental study at 350 degrees C, 500 bars. Geochimica et Cosmochimica Acta 62, 949–960.

Stern, R.J., Fouch, M.J., Klemperer, S., 2003. An overview of the Izu-Bonin-Mariana Subduction Factory. AGU Geophysical Monograph 138, 175–222.

Taylor, B., Martinez, F., 2003. Backarc basalt systematics. Earth Planetary Science Letters 210, 481–497.

Taylor, S.R., McLennan, S.M., 1985. The Continental Crust: Its Composition and Evolution. Blackwell Scientific Publications, Oxford.

Winchester, J.A., Floyd, P.A., 1976. Geochemical and magma type discrimination: application to altered and metamorphosed basic igneous rocks. Earth Planetary Science Letters 28, 459–469.

Windley, B.F., Kröner, A., Xiao, W., 2004. The tectonic evolution of central Asia. In: Jahn, B.-m. (Ed.), International Workshop on Accretionary Orogens and Continental Growth. Abstract vol. National Taiwan University, Tapei, Taiwan, pp. 91–93.

Wu, F., Jahn, B.-m., Wilde, S., Sun, D., 2000. Phanerozoic crustal growth; U–Pb and Sr–Nd isotopic evidence from the granites in northeastern China. Tectonophysics 328, 89–113.

Wu, F., Sun, D., Li, H., Jahn, B.-m., Wilde, S., 2002. A-type granites in northeastern China; age and geochemical constraints on their petrogenesis. Chemical Geology 187, 143–173.

Xiao, W., Windley, B.F., Badarch, G., Sun, S., Li, J., Qin, K., Wang, Z., 2004. Paleozoic accretionary and convergent tectonics of the southern Altaids: implications for the growth of Central Asia. Journal of the Geological Society of London 161L, 339–342.

Xiao, W.J., Windley, B.F., Hao, J., Zhai, M.G., 2003. Accretion leading to collision and the Permian Solonker suture, Inner Mongolia, China: termination of the central Asian orogenic belt. Tectonics 22, 1069. doi:10.1029/2002TC001484.

Yakubchuk, A.S., 2002. The Baikalide-Altaid, Transbaikal-Mongolian and North Pacific orogenic collage: similarity and diversity of structural patterns and metallogenic zoning. In: Blundell, D.J., Neubauer, F., von Quadt, A. (Eds.), The Timing and Location of Major Ore Deposits in an Evolving Orogen, Geological Society of London, vol. 204. Special Publication, pp. 273–297.

Zonenshain, L.P., Suetenko, O.D., Jamyandamba, L., Eenjin, G., 1975. Structure of the axial part of South Mongolian eugeosyncline in the Dzolen Range. Geotectonics 4, 28–44.